Receptor stoichiometry predicts artery-typical vulnerability to altered Notch signaling during smooth muscle differentiation.

Sami Sanlidag[1,2,3], Noora Virtanen[1,2,3,a], Hesam Hoursan[4,5,a], Tommaso Ristori[4,5], Marika Sjöqvist[1,2], Sandra Loerakker[4,5], Cecilia Sahlgren[1,2,3,4,5,6]

[1]Faculty of Science and Engineering, Cell Biology, Åbo Akademi University, Tykistökatu 6, FI-20520, Turku, Finland
[2]Turku Bioscience, Åbo Akademi University and University of Turku, Tykistökatu 6, FI-20520, Turku, Finland
[3]InFLAMES Research Flagship Center, Åbo Akademi University and University of Turku, Turku, Finland
[4]Department of Biomedical Engineering, Eindhoven University of Technology, PO Box 513, 5600 MB, Eindhoven, the Netherlands
[5]Institute for Complex Molecular Systems (ICMS), Eindhoven University of Technology, Ceres, Building Number 7, De Zaale, 5612 AJ, Eindhoven, the Netherlands
[a] These authors contributed equally.
[6]Lead contact. Requests for further information and resources should be directed to and will be fulfilled by the lead contact, Cecilia Sahlgren (Cecilia.sahlren@abo.fi).

Keywords:
Notch signaling, vascular smooth muscle, artery development

ABSTRACT

Jagged1-Notch2 and –Notch3 signaling are important for smooth muscle cell (SMC) development. However, a comprehensive understanding of the Jagged1-Notch2/3 signaling in SMCs has been missing. By combining *in vitro*, *in vivo*, and *in silico* analyses, we here show that Notch2 and Notch3 have overlapping roles in differentiating SMCs upon Jagged1 interaction. However, Notch3 is a less potent inducer of Notch signaling activity compared to Notch2, due to weaker interactions between the Notch3 intracellular domain and RBPJκ. Accordingly, unlike Notch3, Notch2 depletion causes an almost total loss of Notch activity and differentiation in large arteries. In smaller arteries, the loss of Notch2 is partially compensated for by a higher SMC expression of Notch3. Our results, therefore, indicate that SMCs have artery-typical vulnerability to altered Notch2 and Notch3 signaling, contributing to our mechanistic understanding of the Notch-related vascular disease onset.

HIGHLIGHTS

- Notch2 and Notch3 have overlapping functions in vascular smooth muscle cells when activated with Jagged1.
- Notch3 is a weak potentiator of canonical Notch signaling due to lower association between its ICD and RBPJκ compared to Notch2.
- Notch3 can partially compensate for Notch2 depletion in smaller arteries where it is expressed in high quantities.

INTRODUCTION

Vascular smooth muscle cells (SMCs) form a multilayered wall around the endothelium in larger caliber blood vessels, such as arteries, arterioles, and veins, ensuring vascular integrity and function. The dysregulation of SMC development is linked to severe vascular complications and constitutes high clinical significance. However, our understanding of the mechanisms regulating the SMC differentiation in different arteries is incomplete, hindering the development of appropriate therapies for SMC-related pathologies.

During development, vascular SMCs proliferate and produce the extracellular matrix around the endothelium[1,2], followed by SMC maturation. The mature SMCs are contractile and contribute to the vascular tone. In case of alterations in the vascular environment, they can switch between varying phenotypes to partake in vascular adaptation through several mechanisms, including proliferation[3]. Notch signaling, a contact-dependent cell-cell signaling pathway, is a master regulator of SMC development and homeostasis[4]. In mammals, Notch signaling comprises four transmembrane Notch receptors (Notch1, 2, 3, and 4) and five ligands (Jagged1 and 2; and Delta-like 1,3, and 4). When a ligand pulls on a Notch receptor, the receptor becomes poised for two consequent cleavages mediated by ADAM (S2 cleavage) and γ-secretase (S3 cleavage), respectively. This liberates the active Notch intracellular domain (NICD) that can translocate to the nucleus and drive transcription through its co-factors, such as RBPJκ[5,6]. Generally, the receptor-ligand interactions between two juxtaposed cells (trans-interactions) activate the receptor, while those on the same cell (cis-interactions) are considered inhibitory[7]. Notch signaling drives the specification and expansion of SMCs by regulating platelet-derived growth factor receptor β (Pdgfrβ) levels[8,9], as well as their maturation by controlling contractile gene expression and quiescence[10,11]. Furthermore, it propagates around the endothelium through a mechanism called lateral induction, where the Notch activity driven by the endothelial Jagged1 leads to the expression of the SMC-intrinsic Jagged1, which activates Notch in the surrounding cells, thereby contributing to the vascular wall assembly[12–14].

Vascular SMCs mainly express receptors Notch2 and Notch3 and ligand Jagged1. Dysregulation of these molecules can cause vascular complications affecting different vessels in the arterial tree. Alagille syndrome (ALGS) is a congenital disorder attributed to mutations in Jagged1 and, less frequently, Notch2[15]. It manifests with multisystem complications, including intracranial hemorrhages and aneurysms[16–18]. Notch3 is linked to perivascular complications in pulmonary hypertension, such as hypermuscularization and stenosis[19]. Cerebral autosomal dominant arteriopathy with subcortical infarcts and leukoencephalopathy (CADASIL) is caused by mutations on Notch3 and manifests with dementia and smooth muscle loss in smaller caliber arteries and arterioles[20,21]. Similarly, transgenic animals with depletion of these proteins show perivascular pathology. Mice with endothelial cell-specific knockout of Jagged1 are deficient in SMCs and die early during embryonic development[22]. Notch2 knockout mice show abnormalities such as attenuated contractile marker expression and structural defects in the larger elastic pulmonary arteries and aorta, as well as significantly increased rates of patent ductus arteriosus (failure in the closure of the ductus arteriosus) and mortality shortly after birth[10,23,24]. Notch3 knockout does not cause a lethal periarterial phenotype in the developing mouse, apart from mild reduction in the late contractile markers[25,26] and later defects in the myogenic tone and SMC

distribution in small vessels, such as those in the tail and the brain[27–29]. However, the combined knockout of Notch2 and Notch3 is embryonically lethal due to severe perivascular defects, implying overlapping functions between the two receptors[10]. There is also evidence supporting opposing roles for Notch2 and Notch3 in vascular SMC growth and homeostasis. Notch3 promotes proliferation and survival in concert with the ERK signaling[30] *in vitro,* and its elevated activity is linked to the overgrowth of SMCs during pulmonary hypertension[19] and in the aorta of elastin-null mice[31]. Meanwhile, Notch2 promotes cell cycle arrest by p27 stabilization[11]. Despite these indications, a systematic comparison of how Jagged1 signals through Notch2 and Notch3 to regulate different cellular processes during vascular SMC development has been missing.

In this work, we sought to understand the signaling mechanism involving Jagged1, Notch2, and Notch3 and how they regulate SMC differentiation in different arteries in the body. First, using *in vitro* assays and whole transcriptome analysis, we found that Notch2 and Notch3 co-regulated transcriptional programs relating to periarterial development following Jagged1 induction in a time-dependent manner. However, the two receptors differed in their ability to potentiate transcription. Notch2 and Notch3 responded similarly to Jagged1 at the protein level, but Notch2 ICD was transcriptionally more robust, while Notch3 could reach substantial transcriptional activity only when it was highly expressed. Furthermore, through *in situ* hybridization and single-cell transcriptomic databases, we found that SMCs at different arteries varied highly in Notch3 expression. By integrating these findings into a computational model of Notch signaling in arteries, we predicted artery-typical vulnerability to altered Notch signaling in the SMCs, where hypoactivity of Notch2 and Jagged1, but not of Notch3, severely affected Notch signaling. However, SMCs of the arteries with high levels of Notch3 and Jagged1 were predicted to be less dependent on Notch2. Contractile gene reporter assays in zebrafish larvae injected with Notch2 and Notch3 morpholinos recapitulated these predictions, showing that Notch3 can compensate for Notch2 depletion in SMCs of the cerebral vessels that express high levels of Notch3. Overall, our work corroborates the previous *in vivo* findings from the Notch transgenic animals and provides clues for how the altered Notch signaling dosing due to the dysregulated Jagged1-Notch2 and -Notch3 axes can contribute to human periarterial disease onset with local specificity.

RESULTS

Notch2 and Notch3 act as functional analogs during Jagged1-mediated vascular smooth muscle differentiation, but Notch2 is more robust.

To systematically address the functions of Notch2 and Notch3 in the Jagged1-mediated SMC phenotypic regulation, we chose an *in vitro* experimental approach and used immobilized recombinant human Jagged1-Fc dimeric proteins (J1-Fc) to activate the Notch signaling in human aortic SMCs followed by bulk RNA sequencing (Figure 1A). First, we silenced Notch2 or Notch3 in the SMCs using siRNAs (siN2, siN3). 48h post-transfection, Notch2, and Notch3 protein levels were significantly reduced compared to the cells transfected with the non-targeting control (siC) (Figure 1B), suggesting successful silencing of the receptors. We saw a slight reduction in the Notch3 levels (approximately 30 percent) with siN2, but this was expected since Notch3 is a transcriptional target of Notch2[10]. We then grew the cells on immobilized J1-Fc and lysed them for RNA extraction at two different time points. We chose 4 hours and 24 hours, where we expected an early and more Notch-specific transcriptional response to the ligand induction and a later response relating to the SMC differentiation program, respectively. By setting thresholds of fold change (FC) >2 and false discovery rate (FDR) <0.05, we identified 78 genes at 4h (47 up- and 31 downregulated) and 583 genes at 24h (249 up- and 334 downregulated) differentially regulated by Jagged1 induction (see Supplementary Data Table S1 for a complete list of the differentially regulated genes (DEGs)). The top 10 up- and downregulated genes are annotated in Figure 1C.

At 4h, we focused on the upregulated genes, since they would be more directly regulated by the Notch receptor activation. As expected, these included many putative Notch targets, such as HEY1, HEYL, HES1, NRARP, and JAG1. Additionally, we found that genes related to perivascular identity (KCNE4[32]) and SMC quiescence (CDKN2B[33]), as well as TGFβ signaling effectors TGFB3 and SMAD3, were among the upregulated. Interestingly, the silencing of Notch2 and not of Notch3 led to a dramatic loss of transcriptional response to Jagged1, as evidenced by the overall behavior of the gene cluster across the groups (Figures 1D and E). This pattern was reflected in many of the Notch targets, such as HEY1 and NRARP (Figure 1G). Only a few genes, such as KCNE4 and TGFB3 (Figure 1H), seemed to be affected by Notch3 depletion to a similar degree to Notch2.

At 24h, the transcriptional response was more convoluted. Hence, for easier interpretation, we divided the DEGs at 24h into five Ward clusters (2 up- and 3 downregulated clusters) based on how they behaved with Notch2 and Notch3 silencing. Both upregulated clusters, *c,* and *d*, were enriched for ontology terms related to vasculogenesis and myogenic processes, while the three downregulated clusters, *a*, *b,* and *e* were enriched for vascular process-, synaptic signaling-, and cell cycle-related terms, respectively (Figure 1H). Notch2 depletion led to a profound impact on the ligand-induced transcriptomic profile at 24h, which was evident in all five clusters. On the other hand, unlike at 4h, Notch3 silencing seemed to have a consistent (albeit modest compared to Notch2) contribution to the response to Jagged1. Overall, many genes responded strongly to Notch2 already at 4h, while the activity of Notch3 only added to this response at 24h. This pattern was reflected in many genes in *cluster c*, including Notch targets NRARP, HEY1 (Figure 1G), and HEY2; the Jagged1 and Notch3 interactor SDC2[34]; perivascular marker PDGFRB (Figure S1); integrin subunits ITGA1, ITGA11 and ITGB3 (Figure S1) and extracellular matrix components

156 EMILIN2, COL5A3 and COL5A1 (Figure S1). Nonetheless, there were still genes in this cluster
157 that seemed to be affected only by the silencing of Notch2 silencing, such as SNAI2 (Figure S1),
158 which is an important transcription factor for the recruitment of mural progenitors around the aorta
159 from the sclerotome[35]. Additionally, *cluster a,* which seemed to be downregulated mainly by
160 Notch2, included genes such as SOST, RGS2, and EDNRB, which are zonation-specific markers
161 in the pulmonary-aortic tree[36], and genes linked to adverse aortic remodeling, FERMT1, and
162 BMP2[37,38], posing the question of whether Notch2 might be important for the identity of the SMCs
163 at this location.

164 C*lusters d* and *e* (Figure 1E) seemed to be regulated by Notch2 and Notch3 to similar degrees.
165 These clusters were enriched for genes related to the hallmarks of SMC maturation: contractile
166 markers (e.g., ACTA2), extracellular matrix deposition, and cell cycle arrest (e.g., CDKN2B) (See
167 Figure 1F for a longer list of these genes). Interestingly, ACTA2, encoding for the contractility
168 marker α-smooth muscle actin (αSMA), seemed to rely on the activity of both receptors. We
169 wondered whether Notch dosing-sensitive mechanisms could contribute to this effect since Notch
170 signaling can both activate and inhibit the expression of ACTA2. It has been shown that NICD can
171 directly bind the ACTA2 promoter, while HEY inhibits the activity of serum response factor (SRF),
172 which is a gatekeeping transcription factor for contractility-related genes[39–42]. Upon a closer look
173 at our hits, we identified a few genes that were shown to regulate contractile gene expression,
174 OLFM2[43,44], SPON2[45], and FOXS1 in cluster *c*. Among these, the Forkhead box family gene
175 FOXS1 was highly responsive to Jagged1 induction and was among the top DEGs at both 4h and
176 24h. It was regulated only by Notch2 at 4h, and both by Notch2 and Notch3 at 24h, representative
177 of the overall DEG profile in our dataset (Figure S1B). FOXS1 was previously shown to localize
178 in periarterial cells[46,47] and regulate TGFβ-mediated ACTA2 expression[48]. Consistently,
179 transcription factor co-expression analysis on *cluster d* using ChEA3[49] identified FOXS1 as one
180 of the top candidates upstream of these genes (Figure S1C). To test if FOXS1 could act as a
181 "tipping point" favoring ACTA2 expression during Notch activity, we silenced FOXS1 using siRNAs
182 and plated the cells on immobilized J1-Fc. Obstructing the ligand-induced FOXS1 expression led
183 to a consistent decrease in ACTA2 and CNN1 expression, similar to the silencing of Notch2 and
184 Notch3, while SRF silencing abolished their expression almost completely (Figure S1D). We also
185 tested if TGFβ signaling could act downstream of Notch to favor contractility, given the multiple
186 implications related to this signaling pathway in our dataset. We plated SMCs on immobilized J1-
187 Fc with the gamma-secretase inhibitor DAPT and a wide-spectrum TGFβ receptor family inhibitor
188 SB-431542 (TGFβi). TGFβi effectively inhibited the TGFβ receptor signaling, as measured by the
189 decreased Smad2 phosphorylation, while neither the Jagged1 induction nor DAPT led to a
190 significant change in the phosphorylation of Smad2 (Figures S1E and F). On the other hand,
191 DAPT but not TGFβi led to a dramatic decrease in the levels of αSMA. Consistently, TGFβi did
192 not elicit significant changes in the Jagged1-induced COL1A1 and COL4A1 expression (Figure
193 S1G), suggesting that Notch2 and Notch3 regulated the expression of these molecules
194 independently of TGFβ receptor signaling. These findings suggest that the Jagged1-Notch2 and
195 -Notch3 signaling upregulates pro-contractile genes upstream of SRF that favor contractile gene
196 expression.

197 **The Jagged1-Notch2 axis upregulates Notch3 for the progression of the differentiation**
198 **program.**

199 Considering the delayed contribution of Notch3 to the Jagged1-mediated transcriptional
200 response, we sought to understand the temporal relationship between Jagged1, Notch2, and
201 Notch3 better. As Notch3 was already shown to be positively regulated by the Notch signaling[10,50],
202 we attributed its increased influence at 24h to its upregulation. Indeed, NOTCH3 mRNA was
203 upregulated more than two folds upon ligand induction, whereas NOTCH2 mRNA seemed
204 unchanged relative to the basal conditions (Figure 2A). Interestingly, though, the Jagged1-
205 mediated upregulation of NOTCH3 was nearly entirely lost upon Notch2 silencing. Similarly, the
206 S1-cleaved Notch3 products were significantly downregulated with Notch2 depletion after 72
207 hours of Jagged1 induction (Figure S2A and C), suggesting that the activation of the basal Notch3
208 was not sufficient to potentiate its own expression and that this process instead relied on Notch2
209 activity. To confirm this temporal relationship, we performed DAPT washout experiments, where
210 we grew SMCs on immobilized J1-Fc in the presence of DAPT overnight and removed the inhibitor
211 the next day to allow Notch signaling activation and followed the Notch components over time
212 (Figure 2 B). This way, we also hoped to eliminate any bias on the receptor cleavage that might
213 arise from trypsinization at the time of cell plating on the ligands. First, we checked the protein
214 abundance using the wild-type cells (Figure 2D and E) and confirmed that the signal from S1-
215 cleaved Notch3 products, NTM and NEXT, was upregulated by more than 5-fold starting from 24h
216 (See Figure 2C for the probing method for different Notch bands). On the other hand, the
217 corresponding bands for Notch2 were down by nearly 50% compared to the starting conditions,
218 suggesting that Notch2 might be consumed at a faster rate, possibly due to the absence of similar
219 positive feedforward mechanisms for this receptor. Next, we included SMCs with Notch2 or
220 Notch3 silencing in a similar setting and checked the mRNA levels (Figure 2H). The qPCR results
221 recapitulated the same trends, showing that the effect of Notch3 on Notch target gene expression
222 (HEY1 and JAG1) was negligible at 4h, but became more prominent at 24h, consistent with the
223 nearly 3-fold increase of the NOTCH3 mRNA following the Jagged1-induction (Figure 2G). Again,
224 the upregulation of NOTCH3 at 24h was nearly lost with Notch2 silencing, confirming our findings
225 from the RNAseq. To investigate the relevance of the upregulated Notch3, we also checked the
226 abundance of αSMA and the cell-intrinsic Jagged1, and the ACTA2 and JAG1, HEY1 mRNAs
227 later at 72h (Figure S2A and C, and Figure 2C). αSMA and Jagged1, along with all three mRNAs,
228 showed a negative trend upon Notch3 silencing. Contrary to the indications from the RNAseq,
229 Notch3 did not seem to mediate cell-cycle arrest in the absence of Notch2, suggesting that the
230 initial levels of Notch3 might not be sufficient to potentiate this effect (Figure S2B).

231 Interestingly, HEY1 expression at 72h seemed to decrease compared to 24h, possibly due to the
232 decay of the immobilized ligands over time. We prepared spheroid cultures using only SMCs or
233 SMCs together with human umbilical vascular endothelial cells (ECs) to eliminate extrinsic J1-Fc
234 ligands and instead enforce the native cell-cell Jagged1-Notch signaling. After 72h in culture,
235 silencing either Notch2 or Notch3 led to a similar reduction in the immunostaining of Jagged1
236 (Figure S2D and E), supporting that Notch3 contributes to the long-term Notch signaling response
237 to Jagged1. These results together suggest that the initial Notch signaling “push” by the Jagged1-
238 Notch2 axis is necessary for Notch3 expression, which then boosts and sustains the Notch
239 signaling over a prolonged time during *in vitro* SMC differentiation (See Figure 2H for the
240 schematic description of the proposed mechanism).

Elevated levels of Notch3 are required for transcriptionally meaningful canonical Notch3 signaling due to the weak Notch3-CSL interaction.

Next, we wondered why Notch3 relied on amplified expression to produce a sufficient transcriptional response to Jagged1. First, we checked the expression of Notch2 and Notch3 in the SMCs from our RNAseq data. NOTCH3 was expressed nearly twice as much as NOTCH2 already at the basal levels, eliminating the possibility that the difference in activity was caused by the initial levels (Figure S3A). Evidence suggests that the interactions between Jagged1 and Notch3 rely on additional molecules in SMCs[34,51,52]. Hence, we asked whether receptor discrimination by J1-Fc could contribute to the weaker signaling from the Jagged1-Notch3 axis. To test this, we used a saturating concentration (10nM) of pre-labeled soluble J1-Fc to stain live SMCs (Figure 3A). Confocal imaging following the fixation of the stained SMCs showed that silencing of Notch2 and Notch3 caused a visible difference in the fluorescent puncta (Figure 3B). Then, we repeated the live staining protocol and measured the fluorescence signal using FACS. Again, depletion of either receptor caused a comparable shift in the fluorescence profile of the cell populations (Figure 3C). We saw a marginally larger, albeit statistically insignificant, decrease in the mean fluorescence intensity of the Notch2-silenced cells (Figure 3D). We attributed this difference to the slight reduction of Notch3 observed with the Notch2 siRNA. Thus, we concluded that the total interaction of the J1-Fc with Notch2 and Notch3 was comparable. We also investigated the receptor processing triggered by the immobilized J1-Fc at 4, 24, and 72 hours post-DAPT washout due to the evidence that the Notch paralogs vary in sensitivity to cleavage[53–56]. We did not find meaningful differences between Notch2 and Notch3 processing, measured by the ratio of the NEXT to the total signal from the NEXT and the NTM bands (Figure 3E and F). These results together suggested that the large difference in the transcriptional activity of the two receptors could not be explained by J1-Fc binding preference or the differential regulation of receptor processing. Then, we asked whether the intracellular domains of the two receptors could signal at different rates with RBPJκ. We tested this by expressing increased concentrations of NICD2 and NICD3 constructs bearing Flag tags, together with a 12xCSL-Luciferase reporter and β-galactosidase in HEK 293T cells (Figure 3G and H). NICD2 mediated dramatically higher reporter activity, reaching far beyond the dynamic range of NICD3 even at very low concentrations. To test the interaction between the NICD paralogs and RBPJκ, we co-expressed 6xHis-tagged RBPJκ and one of the three NICD paralogs (NICD 1,2, and 3) in HEK 293T cells and performed co-immunoprecipitation using beads bearing α-Flag antibody. Western blot and densitometry analyses showed that NICD1 and NICD2 interacted more strongly than NICD3 with RBPJκ (Figure 3I and J).

Next, we adopted computational modeling to test our hypothesis that the qPCR results can be explained by a stronger transcriptional activity in response to the Notch2-, compared to Notch3-, Jag1 interaction. The computational model, extended from previous versions[13,14] to include both Notch2 and Notch3 signaling (Figure S3B and C), could successfully replicate the qPCR data from Figure 2G (the data at 24h), but only when assuming that NICD2 had a much higher potential to drive JAG1 and NOTCH3 expression than NICD3. Based on the optimization, the algorithm predicted that NICD2 would exert a significantly larger influence, more than two times greater, on the production rates of Notch3 and Jagged1 compared to NICD3 (Figure S3D and F).

These results are also in agreement with the previous literature. Our lab has previously shown that the RAM domain of NICD1 has a much lower dissociation constant (K_d=0.022 μM) than NICD3 (K_d=0.187 μM) for RBPJκ, implying higher affinity between NICD1 and RBPJκ[57]. Furthermore, NICD1 and NICD2 were shown to be functionally interchangeable during murine development and carcinogenesis[53,58]. Thus, these results suggest that the weak transcriptional consequence of the Jagged1-Notch3 axis is caused by the lower potency of the Notch3 ICD to drive RBPJκ-mediated transcription and that higher levels of Notch3 are needed for meaningful Notch signaling output during SMC differentiation.

Levels of Notch3 predict artery-typical vulnerability to altered Jagged1-Notch2/Notch3 signaling in the SMCs.

Next, we wondered if the levels of Notch2 and Notch3 in arterial SMCs vary since the dysregulation of their activities has consequences for different arteries *in vivo*. Notch3 expression in the outflow tract was suggested to depend on the embryonic lineage, where the SMCs of the neural crest origin show higher Notch3 expression than those derived from the sclerotome and the second heart field[25]. Hence, we checked the expression of Notch signaling components in the arterial cells from multiple locations using previously published single-cell RNAseq data from adult mice[36,59,60] (Figure 4A-C). Notch2 expression was relatively low in all arteries and showed little variation. Surprisingly, Notch3 expression varied vastly among the SMCs of different arteries. It was expressed highly in smaller muscular arteries, such as the coronary arteries in the heart and the arteries in the brain, and the colon. Meanwhile, the aorta, the proximal and the distal regions combined, had strikingly little Notch3 in comparison.

Next, we aimed to see how the expression of the two receptors could affect the Notch signaling output in the arterial wall. Using the optimized parameters relating to the Jagged1-Notch2/3 kinetics from our simulations in Figure S3F (also see Table 2 in STAR Methods), we extended the computational model of Notch signaling in the arteries that was previously adapted and tested by our lab[13,61–63] (Figure 4D) to take Notch2 and Notch3 dynamics into account during the Jagged1-mediated lateral induction, and to calculate a "Notch multiplier" (Notch multiplier=1 indicates no Jagged1-mediated Notch activity) as a measure of the Notch signaling activity in a simulated arterial wall. We then adjusted the basal Jagged1, Notch2, and Notch3 production rates in SMCs ($N_2^{pr}, N_3^{pr}, J^{pr}$) in a range between 0 and 3000 h^{-1} to predict the Notch multiplier in different Notch2-Notch3 stoichiometries (Figure 4E). The model was highly sensitive to Jagged1 and Notch2 manipulations, as the Notch multiplier rapidly increased with respect to J^{pr} and N_2^{pr}. Meanwhile, increasing N_3^{pr} had little impact on the Notch multiplier and its contribution was merely additive to that of N_2^{pr}.

To put the Notch multiplier in a physiological perspective, we chose Notch stoichiometries resembling those in different arterial SMCs. Considering the low expression of Notch2 and the relatively higher Notch3 expression in all arterial SMCs, we assigned $Notch2^{Low}/Notch3^{Low}$ (N_2^{pr}= 500 h^{-1}, N_3^{pr} = 1000 h^{-1}) and $Notch2^{Low}/Notch3^{High}$ stoichiometry (N_2^{pr}= 500 h^{-1}, N_3^{pr} = 3000 h^{-1}) for aortic and pulmonary SMCs, respectively. For Jpr, we set the minimum physiological threshold to 1000 h^{-1}, since otherwise, the Notch multiplier was not meaningful with the chosen ranges of N_2^{pr} and N_3^{pr}. For the muscular arterial SMCs (coronary, colon, and brain arterial SMCs) we used

the same Notch2^{Low}/Notch3^{High} stoichiometry but set the J^{pr} to 3000 h^{-1} in line with the higher Jag1 expression seen in these cells. This way, we could fit the numbers representative of different arterial SMCs within the dynamic range of our simulations (Figure 4F). This approach yielded Notch multiplier values resembling the trend of Nrarp expression across different arterial SMCs (Figure 4C). Furthermore, setting Jpr to 0 with the aortic receptor parameters reduced the Notch multiplier from 2.24 to nearly 1 (Figure S3G), resulting in a similar negative 2-fold change that was seen with Notch target gene expression in the mouse aortic smooth muscle upon Jagged1 knockout[64].

Next, we explored knockout scenarios for Notch2 or Notch3 by setting the production rates of either to 0. The model predicted that Notch2 knockout, but not Notch3 knockout, would dramatically reduce the Notch multiplier in all arterial conditions (Figure 4E). Setting N2pr to 0 resulted in an approximately 2-fold decrease in the Notch multiplier in the aortic SMCs (2.24 to 1.12), leading to almost a complete loss of the Notch activity. Although the pulmonary SMCs expressed three times as much Notch3, the decrease in the Notch multiplier with Notch2 knockout was comparable with the aortic SMCs (2.02 to 1.33), consistent with the importance of Notch2 in the outflow tract. The Notch multiplier in the muscular arterial SMCs, which expressed 3 times as much Notch3 and Jag1 as their aortic counterparts, was reduced from 4.61 to 1.73 with Notch2 knockout. However, we observe that a Notch multiplier of 1.73 is reasonably close to the Notch multiplier that the model predicted for the aorta and the pulmonary arteries in the basal conditions. Thus, one can argue that this level of Notch activity might be sufficient for SMC development. These results suggest that elevated expression of Notch3 in these arteries can partly compensate for Notch2 depletion, provided high basal Jagged1 expression in the SMCs. Since the periarterial Notch signaling is initiated via ECs[12,65], we also checked Jag1 expression in these cells from the same scRNA datasets. The ECs of the muscular arteries did not show elevated Jag1, unlike the SMCs (Figure 4B). However, ECs express high levels of Dll4 (Figure 4B), which was shown to contribute to the signaling between the coronary endothelium and the developing SMCs[66]. Thus, Dll4 and Jagged1 could help induce sufficient Notch signal in the first layer of SMCs to kickstart lateral induction in the developing media. Supporting this notion, mice with SMC-specific knockout of Jagged1 develop an SMC layer adjacent to the endothelium in the descending aorta, but this layer is much thinner compared to the wildtype, highlighting the importance of Jagged1 of the SMC-origin[67].

Overall, our model predicts that Notch3 depletion has a negligible impact on the periarterial Notch signaling, but that Notch2 depletion is highly detrimental, especially for the aortic-pulmonary tree. Furthermore, it predicts that high expression of Notch3 can partly compensate for Notch2 depletion, but the compensatory effect of Notch3 is dependent on sufficient expression of Jagged1, highlighting the importance and the dose sensitivity of this ligand during periarterial development.

Artery-typical elevated Notch3 expression in the developing SMCs can compensate for Notch2 depletion in the zebrafish larvae.

We wondered if we could capture the reliance on Notch2 and/or Notch3 based on their stoichiometry *in vivo* in a developmental setting. For this purpose, we chose zebrafish larvae, an established model for vascular development[68]. Notch2 and Notch3 knockout zebrafish larvae

were already shown to have a reduced number of the perivascular precursors in the dorsal aorta (DA), and the cerebral base arteries, BCA (basal communicating artery) and PCS (posterior communicating segment), respectively[9]. Thus, we started by assessing the Notch receptor expression in the developing zebrafish perivascular cells in these locations (Figure 5A). There are no reliable antibodies for the zebrafish Notch receptors; thus, we performed *in situ* Hybridization Chain Reaction (HCR) in 3dpf larvae expressing a pdgfrb reporter using probes against notch2 and notch3. We could not reliably quantify the total intensity or the number of the mRNA puncta per cell, due to the difficulty of segmenting the pdgfrb^{High} cells and the diffuse signal from notch3. However, notch3 was stained more consistently and colocalized with the pdgfrb reporter in broader areas in the cerebral base, while the staining was sparser in the dorsal aorta. On the other hand, notch2 was stained similarly sparsely in the cerebral base and the dorsal aorta (Figure 5B and C).

Next, for a more quantitative approach, we turned to a single-cell RNAseq dataset from Zebrahub[69]. Here, we chose to look at the mesoderm dataset, since mural progenitors at the cerebral base and the dorsal aorta mainly derive from this lineage[70]. We extracted the cell cluster, compiling all SMCs under the annotation “visceral muscle”. We created UMAP projections using the Seurat package[71] (Figure 5D) and identified the vascular SMC clusters by sorting out the cells expressing non-vascular SMC markers desmb, nrg1, and nkx2.3 (Figure S4). Among the remaining, the clusters #3, #9, and #11 from the 3dpf (days post-fertilization) and the clusters #0, #1, and #7 from 5- and 10dpf larvae were positive for the SMC markers acta2, tagln, and myh11a (Figure S4). We excluded the cells from the earlier developmental stages since the mural cells emerge around 2dpf and express little contractility markers until 3dpf[9]. Out of these clusters, cluster #9 and cluster #3 expressed dramatically higher levels of notch3 compared to the others, and showed higher pdgfrb and foxc1 expression typical of the cerebral SMCs[72], along with pericyte-associated genes zeb2a, rasl12, and ednraa (Figure 5E and Figure S4), consistent with the pericyte-like properties of the SMCs in the smaller cerebral[73] and coronary arteries[26]. Moreover, these cells were negative for spatially restricted homeobox genes, such as hoxc1a[74], unlike the other SMC clusters, suggesting that they are from vessels anterior to the hindbrain. They also showed higher levels of jag1b and a notch2^{Low}/notch3^{High} stoichiometry (Figure 5C), recapitulating the same expression pattern as the murine brain SMCs.

Finally, to test whether elevated notch3 could drive the differentiation of these cells without the need for notch2, we injected embryos bearing tagln and kdrl reporters with notch2 or notch3 morpholinos. Light sheet microscopy at 102 hpf (hours post-fertilization) revealed that the notch2 morphants had a significantly decreased number of tagln+ objects around their dorsal aorta, whereas the notch3 morphants were indistinguishable from the control fish, supporting the negligible contribution of notch3 to SMC differentiation in this location (Figure 5G and H). At BCA and PCS, we could not detect any differences between the notch2 morphants and the control. However, consistent with the loss of the pdgfrb+ perivascular progenitor emergence in this location with notch3 knockout[9], the notch3 morphants showed a negative trend in the number of tagln+ objects (Figure 5G and H). Overall, these results suggested that artery-typical elevated Notch3 expression could compensate for Notch2 depletion during SMC differentiation in the developing zebrafish, corroborating our simulated results.

DISCUSSION

409 Notch signaling is integral in perivascular cell specification, maturation, and homeostasis. As a
410 result, its dysregulation is linked to congenital and acquired diseases with catastrophic
411 consequences for the vasculature. In this work, we set out to study the signaling mechanism
412 governing Jagged1 and the receptors Notch2 and Notch3 and how it regulates arterial SMC
413 development. Our findings support a causal role of Notch2 for Notch3[10]. Furthermore, we show
414 that when induced with Jagged1, Notch2 and Notch3 both regulate genes related to vascular
415 SMC specification, maturation, and quiescence, albeit with lower transcriptional activity by
416 Notch3. This supports the previous notion that the two receptors could essentially be mutually
417 compensatory during SMC development[9,10]. We cannot state that Notch2 and Notch3 specifically
418 regulate different genes without NICD-DNA interaction assays, such as ChIPSeq, especially given
419 the temporal relationship between Notch2 and Notch3. However, we do not exclude the possibility
420 that they might otherwise have specific targets that are not directly related to SMC differentiation,
421 considering the genes associated with the pulmonary-aortic tree regulated by Notch2 in our
422 RNAseq data. As for Notch3, we could not detect any specific markers among the Jagged1-
423 induced genes that would suggest a pro-growth function, as previously suggested[30]. Therefore,
424 the canonical Jagged1-Notch3 signaling does not directly explain the effects, such as the
425 pathological SMC growth during pulmonary hypertension. However, Notch3 might have
426 paradoxical functions due to non-canonical mechanisms independent of Jagged1. Indeed, it was
427 shown to be constitutively active without ligand induction and promote cell growth in basal breast
428 cancer[75]. Therefore, in a perivascular context, one must carefully consider whether a particular
429 effect is linked directly to the Jagged1-Notch3 axis or the increased cell-autonomous functions of
430 Notch3 following its upregulation as a target of Notch signaling itself.

431 We show that the Jagged1-Notch3 axis is weaker in inducing a transcriptional response compared
432 to Notch2 and relies on the high abundance of both Jagged1 and Notch3. This has the following
433 implications for the Notch-related vascular disease context. First, the low canonical activity of
434 Notch3 would imply a heavier burden on the Jagged1-Notch2 axis during smooth muscle cell
435 development than previously thought, especially for those in the aorta, where Notch3 is expressed
436 in lower quantities compared to the smaller arteries. This is consistent with the severe
437 deformations observed in the outflow tract of mice with Notch2 and/or Jagged1 depletion, such
438 as patent ductus arteriosus[24] and aortic narrowing[23]. Similarly, ALGS patients frequently present
439 narrowing defects in the outflow tract, such as pulmonary stenosis and aortic coarctation[16,18].
440 Conflicting evidence suggests that the induced knockout of Notch2 in adult mice does not affect
441 the neointimal area following carotid injury[76] or diet-induced atherosclerotic plaque formation[77].
442 However, Notch2 activity might be more integral during the development of SMCs than in their
443 homeostasis or injury response, since in the latter case, the perivascular tissue is already
444 established and rich in supporting extracellular matrix that can switch on compensatory
445 mechanisms. Indeed, loss of elastin in the aorta causes epigenetic activation of Notch3
446 expression[31], which might provide sufficient Notch signaling input in case of periarterial injury.

447 Second, due to the low transcriptional contribution of Notch3, our results indicate that perivascular
448 defects related to the dysregulation of the Jagged1-Notch3 axis (e.g., in CADASIL) might be
449 associated with the sustainment of the differentiated SMC state and homeostasis, rather than
450 early SMC development. Consistently, the late contractile SMC marker Myh11, but not the SMC
451 precursor emergence is affected by Notch3 depletion in the mouse heart[26]. Additionally, there is

growing consensus that the molecular mechanism underlying the poor SMC coverage in CADASIL is the abnormal accumulation of the Notch3 ECD on the cell surface due to the obstruction of its ligand-dependent elimination, pointing at a gain-of-function effect of Notch3 rather than defective Notch3 signaling[78–81]. A Jagged1 mutation in mice phenocopying the human ALGS (Jag1^{Ndr}) shows partial loss in its binding capacity to Notch3 ECD[82] and causes poor SMC coverage in the retinal arterioles and the coronary arteries with increased SMC apoptosis[83] similar to CADASIL, asking whether this phenotype links to a defect in the Notch3 ECD elimination. Here we show that smaller muscular arteries like those in the brain and the heart express elevated levels of Notch3, which could boost Notch3 ECD accumulation in these locations and contribute to the small vessel specificity of CADASIL. Indeed, mutant Notch3 (R169C) does not cause a change in the expression of Notch3-driven genes in the arteries, but the forced expression of two copies of the mutant in addition to the wildtype Notch3 exacerbates the ECD accumulation and the resulting arteriopathy. Meanwhile, eliminating one copy of the wildtype Notch3 alleviates the phenotype[84], supporting a Notch3 overdose mechanism over a Notch3 hypo-signaling scenario. Additionally, we have previously shown that Notch3 and Jagged1, but not Notch2, were negatively regulated by strain[13,85]. Thus, it is likely that altered hemodynamics, like high blood pressure, has a considerable impact on how Notch3 functions in smaller arteries during disease. Overall, the differences in the transcriptional influence of Notch2 and Notch3, and the artery-typical variations in their stoichiometry can partly explain the locally restricted periarterial phenotypes and clinical findings relating to dysregulation of Jagged1, Notch2, and Notch3.

LIMITATIONS OF THE STUDY

This study has several limitations. Most importantly, our findings are based on the mRNA level expression, and thus, we cannot dismiss the possibility that Notch2 and Notch3 are regulated differently at the protein level, affecting how many of these receptors end up on the membrane. Indeed, contrary to our predictions, Notch3 knockout alone causes an almost complete loss of perivascular cells in the cerebral base of zebrafish larvae[86], showing that Notch2 cannot compensate for Notch3 depletion in this location. While we found that all vascular SMC clusters in zebrafish larvae expressed comparable levels of Notch2 based on Zebrahub, in reality, only a small fraction of the cells in the cerebral arteries were found to be positive for Notch2 reporter activity[86]. Thus, we acknowledge the need for tools to assess different Notch protein levels and say whether some cells might rely solely on Notch3. Additionally, Notch targets respond differently to the temporal abundance of NICD[87] and might be regulated by co-transcriptional factors in addition to RBPJκ[88]. Notch3 might bind the promoters of contractility-related genes more efficiently than the other putative Notch targets, as implied by our RNAseq data. Thus, we cannot exclude the possibility that the transcriptional influence of Notch3 might be higher than our predictions. Indeed, cerebral-enriched Foxc1 boosts NICD activity in the zebrafish[89].

AUTHOR CONTRIBUTIONS

SS, MS, and CS conceptualized the work. SS, NV, HH, and TR designed the experiments. SS, NV, HH, and TR executed the experiments, analyzed the data, and prepared the figures. SS wrote the initial draft. SS, NV, HH, TR, MS, SL, and CS revised and edited the draft. TR, MS, SL, and CS supervised the study. TR, SL, and CS acquired funding for the study.

FUNDING

This project has received funding from the European Research Council (ERC) and the European Union's Horizon 2020 research and innovation program under grant agreement No. 771168 (ForceMorph) and the European Research Council (ERC) grant agreement No. 802967 (MechanoSignaling). The research has also been supported by the Academy of Finland, decision numbers #316882 (SPACE), #330411 (SignalSheets), #336355 (Solutions for Health at Åbo Akademi University) and #337531 (InFLAMES Flagship Programme). We have also received funding from the Swedish Cultural Foundation, the Finnish Cultural Foundation, the Sigrid Juselius Foundation, Åbo Akademi University Foundation's Centers of Excellence in Cellular Mechanostasis (CellMech), Bioelectronic Activation of Cell Functions (BACE) Jane and Aarno Errko Foundation and the Finnish Society of Sciences and Letters.

ACKNOWLEDGEMENTS

The bulk RNA sequencing and the data analysis were done in the Finnish Functional Genomics Center, and the Medical Bioinformatics Center Turku. All zebrafish work was done in Zebrafish Core Facility in Turku Bioscience. All microscopy experiments were done in the Cellular Imaging Core in Turku Bioscience. We would like to thank previous laboratory trainees Amanda Norren and Ana Ayala Perez for their help with the differentiation assays. We also thank other persons for the following: help with laboratory and administrative work (Alexandra Manea), help with the design of the RBPJκ plasmid (Elenaé Vázquez-Ulloa), guidance and help with flow cytometry assays (Ezgi Özliseli), guidance and help with the qPCR assays (Marjaana Parikainen and Kati Kemppainen), guidance and help with light sheet microscopy and image analysis (Markus Peurla and Anna-Mari Haapanen-Saaristo), guidance with zebrafish experiments (Ilkka Paatero), and help with setting up the computational model (Margot Passier).

DECLARATION OF INTEREST

The authors declare no conflicts of interest.

DECLARATION OF GENERATIVE AI AND AI-ASSISTED TECHNOLOGIES

No AI-assisted tools were used during the preparation of this manuscript.

DATA AND CODE AVAILABILITY

The data and the code generated during this study will be made available in an open repository upon the approval of the manuscript for publication.

SUPPLEMENTARY MATERIALS

Figure S1. *Notch2 and Notch3 both act upstream of genes associated with Jagged1-driven periarterial coverage and maturation (Related to Figure 1).*

Figure S2. *Late Notch3 activity is important for the contractile differentiation (Related to Figures 1 and 2)*

Figure S3. *(Related to Figure 3 and Figure 4):*

Figure S4. *(Related to Figure 5)*

Table S1. The Bulk RNAseq DEGs and gene counts

REFERENCES

1. Hellström, M., Kalén, M., Lindahl, P., Abramsson, A., and Betsholtz, C. (1999). Role of PDGF-B and PDGFR-β in recruitment of vascular smooth muscle cells and pericytes during embryonic blood vessel formation in the mouse. Development *126*, 3047–3055. https://doi.org/10.1242/dev.126.14.3047.

2. Wagenseil, J.E., and Mecham, R.P. (2009). Vascular Extracellular Matrix and Arterial Mechanics. Physiological Reviews *89*, 957–989. https://doi.org/10.1152/physrev.00041.2008.

3. Yap, C., Mieremet, A., de Vries, C.J.M., Micha, D., and de Waard, V. (2021). Six Shades of Vascular Smooth Muscle Cells Illuminated by KLF4 (Krüppel-Like Factor 4). Arteriosclerosis, Thrombosis, and Vascular Biology *41*, 2693–2707. https://doi.org/10.1161/ATVBAHA.121.316600.

4. Baeten, J.T., and Lilly, B. (2017). Notch Signaling in Vascular Smooth Muscle Cells. Adv Pharmacol *78*, 351–382. https://doi.org/10.1016/bs.apha.2016.07.002.

5. Siebel, C., and Lendahl, U. (2017). Notch Signaling in Development, Tissue Homeostasis, and Disease. Physiological Reviews *97*, 1235–1294. https://doi.org/10.1152/physrev.00005.2017.

6. Suarez Rodriguez, F., Sanlidag, S., and Sahlgren, C. (2023). Mechanical regulation of the Notch signaling pathway. Current Opinion in Cell Biology *85*, 102244. https://doi.org/10.1016/j.ceb.2023.102244.

7. Sjöqvist, M., and Andersson, E.R. (2019). Do as I say, Not(ch) as I do: Lateral control of cell fate. Developmental Biology *447*, 58–70. https://doi.org/10.1016/j.ydbio.2017.09.032.

8. Jin, S., Hansson, E.M., Tikka, S., Lanner, F., Sahlgren, C., Farnebo, F., Baumann, M., Kalimo, H., and Lendahl, U. (2008). Notch Signaling Regulates Platelet-Derived Growth Factor Receptor-β Expression in Vascular Smooth Muscle Cells. Circulation Research *102*, 1483–1491. https://doi.org/10.1161/CIRCRESAHA.107.167965.

9. Ando, K., Wang, W., Peng, D., Chiba, A., Lagendijk, A.K., Barske, L., Crump, J.G., Stainier, D.Y.R., Lendahl, U., Koltowska, K., et al. (2019). Peri-arterial specification of vascular mural cells from naïve mesenchyme requires Notch signaling. Development *146*, dev165589. https://doi.org/10.1242/dev.165589.

562 10. Wang, Q., Zhao, N., Kennard, S., and Lilly, B. (2012). Notch2 and Notch3 Function
563 Together to Regulate Vascular Smooth Muscle Development. PLOS ONE *7*, e37365.
564 https://doi.org/10.1371/journal.pone.0037365.

565 11. Boucher, J.M., Harrington, A., Rostama, B., Lindner, V., and Liaw, L. (2013). A Receptor-
566 Specific Function for Notch2 in Mediating Vascular Smooth Muscle Cell Growth Arrest
567 Through Cyclin-dependent Kinase Inhibitor 1B. Circulation Research *113*, 975–985.
568 https://doi.org/10.1161/CIRCRESAHA.113.301272.

569 12. Manderfield, L.J., High, F.A., Engelka, K.A., Liu, F., Li, L., Rentschler, S., and Epstein, J.A.
570 (2012). Notch activation of Jagged1 contributes to the assembly of the arterial wall.
571 Circulation *125*, 314–323. https://doi.org/10.1161/CIRCULATIONAHA.111.047159.

572 13. Loerakker, S., Stassen, O.M.J.A., ter Huurne, F.M., Boareto, M., Bouten, C.V.C., and
573 Sahlgren, C.M. (2018). Mechanosensitivity of Jagged–Notch signaling can induce a
574 switch-type behavior in vascular homeostasis. Proceedings of the National Academy of
575 Sciences *115*, E3682–E3691. https://doi.org/10.1073/pnas.1715277115.

576 14. Ristori, T., Stassen, O.M.J.A., Sahlgren, C.M., and Loerakker, S. (2020). Lateral induction
577 limits the impact of cell connectivity on Notch signaling in arterial walls. International
578 Journal for Numerical Methods in Biomedical Engineering *36*, e3323.
579 https://doi.org/10.1002/cnm.3323.

580 15. Gilbert, M.A., Bauer, R.C., Rajagopalan, R., Grochowski, C.M., Chao, G., McEldrew, D.,
581 Nassur, J.A., Rand, E.B., Krock, B.L., Kamath, B.M., et al. (2019). Alagille syndrome
582 mutation update: Comprehensive overview of JAG1 and NOTCH2 mutation frequencies
583 and insight into missense variant classification. Hum Mutat *40*, 2197–2220.
584 https://doi.org/10.1002/humu.23879.

585 16. McElhinney, D.B., Krantz, I.D., Bason, L., Piccoli, D.A., Emerick, K.M., Spinner, N.B., and
586 Goldmuntz, E. (2002). Analysis of Cardiovascular Phenotype and Genotype-Phenotype
587 Correlation in Individuals With a JAG1 Mutation and/or Alagille Syndrome. Circulation
588 *106*, 2567–2574. https://doi.org/10.1161/01.CIR.0000037221.45902.69.

589 17. Emerick, K.M., Krantz, I.D., Kamath, B.M., Darling, C., Burrowes, D.M., Spinner, N.B.,
590 Whitington, P.F., and Piccoli, D.A. (2005). Intracranial Vascular Abnormalities in Patients
591 with Alagille Syndrome. Journal of Pediatric Gastroenterology and Nutrition *41*, 99–107.
592 https://doi.org/10.1097/01.MPG.0000162776.67758.2F.

593 18. Yuan, S.-M. (2022). Pulmonary artery pathologies in Alagille syndrome: a meta-analysis.
594 Postepy Kardiol Interwencyjnej *18*, 111–117. https://doi.org/10.5114/aic.2022.118526.

595 19. Zhang, Y., Hernandez, M., Gower, J., Winicki, N., Morataya, X., Alvarez, S., Yuan, J.X.-J.,
596 Shyy, J., and Thistlethwaite, P.A. (2022). JAGGED-NOTCH3 signaling in vascular

remodeling in pulmonary arterial hypertension. Science Translational Medicine *14*, eabl5471. https://doi.org/10.1126/scitranslmed.abl5471.

20. Okeda, R., Arima, K., and Kawai, M. (2002). Arterial Changes in Cerebral Autosomal Dominant Arteriopathy With Subcortical Infarcts and Leukoencephalopathy (CADASIL) in Relation to Pathogenesis of Diffuse Myelin Loss of Cerebral White Matter. Stroke *33*, 2565–2569. https://doi.org/10.1161/01.STR.0000032620.91848.1C.

21. Joutel, A., Corpechot, C., Ducros, A., Vahedi, K., Chabriat, H., Mouton, P., Alamowitch, S., Domenga, V., Cécillion, M., Maréchal, E., et al. (1996). Notch3 mutations in CADASIL, a hereditary adult-onset condition causing stroke and dementia. Nature *383*, 707–710. https://doi.org/10.1038/383707a0.

22. High, F.A., Lu, M.M., Pear, W.S., Loomes, K.M., Kaestner, K.H., and Epstein, J.A. (2008). Endothelial expression of the Notch ligand Jagged1 is required for vascular smooth muscle development. Proc Natl Acad Sci U S A *105*, 1955–1959. https://doi.org/10.1073/pnas.0709663105.

23. Varadkar, P., Kraman, M., Despres, D., Ma, G., Lozier, J., and McCright, B. (2008). Notch2 is required for the proliferation of cardiac neural crest-derived smooth muscle cells. Developmental Dynamics *237*, 1144–1152. https://doi.org/10.1002/dvdy.21502.

24. Baeten, J.T., Jackson, A.R., McHugh, K.M., and Lilly, B. (2015). Loss of Notch2 and Notch3 in vascular smooth muscle causes patent ductus arteriosus. Genesis *53*, 738–748. https://doi.org/10.1002/dvg.22904.

25. Granata, A., Bernard, W.G., Zhao, N., Mccafferty, J., Lilly, B., and Sinha, S. (2015). Temporal and Embryonic Lineage-Dependent Regulation of Human Vascular SMC Development by NOTCH3. Stem Cells and Development *24*, 846–856. https://doi.org/10.1089/scd.2014.0520.

26. Volz, K.S., Jacobs, A.H., Chen, H.I., Poduri, A., McKay, A.S., Riordan, D.P., Kofler, N., Kitajewski, J., Weissman, I., and Red-Horse, K. Pericytes are progenitors for coronary artery smooth muscle. eLife *4*, e10036. https://doi.org/10.7554/eLife.10036.

27. Domenga, V., Fardoux, P., Lacombe, P., Monet, M., Maciazek, J., Krebs, L.T., Klonjkowski, B., Berrou, E., Mericskay, M., Li, Z., et al. (2004). Notch3 is required for arterial identity and maturation of vascular smooth muscle cells. Genes Dev *18*, 2730–2735. https://doi.org/10.1101/gad.308904.

28. de Chantemèle, E.J.B., Retailleau, K., Pinaud, F., Vessières, E., Bocquet, A., Guihot, A.L., Lemaire, B., Domenga, V., Baufreton, C., Loufrani, L., et al. (2008). Notch3 is a major regulator of vascular tone in cerebral and tail resistance arteries. Arterioscler Thromb Vasc Biol *28*, 2216–2224. https://doi.org/10.1161/ATVBAHA.108.171751.

632 29. Henshall, T.L., Keller, A., He, L., Johansson, B.R., Wallgard, E., Raschperger, E., Mäe,
633 M.A., Jin, S., Betsholtz, C., and Lendahl, U. (2015). Notch3 Is Necessary for Blood
634 Vessel Integrity in the Central Nervous System. Arteriosclerosis, Thrombosis, and
635 Vascular Biology *35*, 409–420. https://doi.org/10.1161/ATVBAHA.114.304849.

636 30. Baeten, J.T., and Lilly, B. (2015). Differential Regulation of NOTCH2 and NOTCH3
637 Contribute to Their Unique Functions in Vascular Smooth Muscle Cells. J Biol Chem
638 *290*, 16226–16237. https://doi.org/10.1074/jbc.M115.655548.

639 31. Dave, J.M., Chakraborty, R., Ntokou, A., Saito, J., Saddouk, F.Z., Feng, Z., Misra, A.,
640 Tellides, G., Riemer, R.K., Urban, Z., et al. (2022). JAGGED1/NOTCH3 activation
641 promotes aortic hypermuscularization and stenosis in elastin deficiency. J Clin Invest
642 *132*. https://doi.org/10.1172/JCI142338.

643 32. Kapuria, S., Bai, H., Fierros, J., Huang, Y., Ma, F., Yoshida, T., Aguayo, A., Kok, F., Wiens,
644 K.M., Yip, J.K., et al. (2022). Heterogeneous pdgfrb+ cells regulate coronary vessel
645 development and revascularization during heart regeneration. Development *149*,
646 dev199752. https://doi.org/10.1242/dev.199752.

647 33. Leeper, N.J., Raiesdana, A., Kojima, Y., Kundu, R.K., Cheng, H., Maegdefessel, L., Toh,
648 R., Ahn, G.-O., Ali, Z.A., Anderson, D.R., et al. (2013). Loss of CDKN2B Promotes p53-
649 Dependent Smooth Muscle Cell Apoptosis and Aneurysm Formation. Arteriosclerosis,
650 Thrombosis, and Vascular Biology *33*, e1–e10.
651 https://doi.org/10.1161/ATVBAHA.112.300399.

652 34. Zhao, N., Liu, H., and Lilly, B. (2012). Reciprocal Regulation of Syndecan-2 and Notch
653 Signaling in Vascular Smooth Muscle Cells *. Journal of Biological Chemistry *287*,
654 16111–16120. https://doi.org/10.1074/jbc.M111.322107.

655 35. Murayama, E., Vivier, C., Schmidt, A., and Herbomel, P. (2023). Alcam-a and Pdgfr-α are
656 essential for the development of sclerotome-derived stromal cells that support
657 hematopoiesis. Nat Commun *14*, 1171. https://doi.org/10.1038/s41467-023-36612-y.

658 36. Muhl, L., Mocci, G., Pietilä, R., Liu, J., He, L., Genové, G., Leptidis, S., Gustafsson, S.,
659 Buyandelger, B., Raschperger, E., et al. (2022). A single-cell transcriptomic inventory of
660 murine smooth muscle cells. Dev Cell *57*, 2426-2443.e6.
661 https://doi.org/10.1016/j.devcel.2022.09.015.

662 37. Ainiwan, M., Wang, Q., Yesitayi, G., and Ma, X. (2022). Identification of FERMT1 and
663 SGCD as key marker in acute aortic dissection from the perspective of predictive,
664 preventive, and personalized medicine. EPMA J *13*, 597–614.
665 https://doi.org/10.1007/s13167-022-00302-4.

666 38. Klessinger, D., Mamazhakypov, A., Glaeser, S., Emig, R., Peyronnet, R., Meier, L.,
667 Proelss, K., Marenne, K., Smolka, C., Grundmann, S., et al. (2024). Divergent and

Compensatory Effects of BMP2 and BMP4 on the VSMC Phenotype and BMP4's Role in Thoracic Aortic Aneurysm Development. Cells *13*, 735. https://doi.org/10.3390/cells13090735.

39. Morrow, D., Scheller, A., Birney, Y.A., Sweeney, C., Guha, S., Cummins, P.M., Murphy, R., Walls, D., Redmond, E.M., and Cahill, P.A. (2005). Notch-mediated CBF-1/RBP-Jκ-dependent regulation of human vascular smooth muscle cell phenotype in vitro. American Journal of Physiology-Cell Physiology *289*, C1188–C1196. https://doi.org/10.1152/ajpcell.00198.2005.

40. Doi, H., Iso, T., Sato, H., Yamazaki, M., Matsui, H., Tanaka, T., Manabe, I., Arai, M., Nagai, R., and Kurabayashi, M. (2006). Jagged1-selective Notch Signaling Induces Smooth Muscle Differentiation via a RBP-Jκ-dependent Pathway *. Journal of Biological Chemistry *281*, 28555–28564. https://doi.org/10.1074/jbc.M602749200.

41. Boucher, J.M., Peterson, S.M., Urs, S., Zhang, C., and Liaw, L. (2011). The miR-143/145 Cluster Is a Novel Transcriptional Target of Jagged-1/Notch Signaling in Vascular Smooth Muscle Cells*. Journal of Biological Chemistry *286*, 28312–28321. https://doi.org/10.1074/jbc.M111.221945.

42. Rozenberg, J.M., Taylor, J.M., and Mack, C.P. (2018). RBPJ binds to consensus and methylated cis elements within phased nucleosomes and controls gene expression in human aortic smooth muscle cells in cooperation with SRF. Nucleic Acids Research *46*, 8232–8244. https://doi.org/10.1093/nar/gky562.

43. Shi, N., Guo, X., and Chen, S.-Y. (2014). Olfactomedin 2, a novel regulator for transforming growth factor-β–induced smooth muscle differentiation of human embryonic stem cell–derived mesenchymal cells. Mol Biol Cell *25*, 4106–4114. https://doi.org/10.1091/mbc.E14-08-1255.

44. Shi, N., Li, C.-X., Cui, X.-B., Tomarev, S.I., and Chen, S.-Y. (2017). Olfactomedin 2 Regulates Smooth Muscle Phenotypic Modulation and Vascular Remodeling Through Mediating Runt-Related Transcription Factor 2 Binding to Serum Response Factor. Arteriosclerosis, Thrombosis, and Vascular Biology *37*, 446–454. https://doi.org/10.1161/ATVBAHA.116.308606.

45. Zhu, L.-H., Huang, L., Zhang, X., Zhang, P., Zhang, S.-M., Guan, H., Zhang, Y., Zhu, X.-Y., Tian, S., Deng, K., et al. (2015). Mindin regulates vascular smooth muscle cell phenotype and prevents neointima formation. Clinical Science *129*, 129–145. https://doi.org/10.1042/CS20140679.

46. Heglind, M., Cederberg, A., Aquino, J., Lucas, G., Ernfors, P., and Enerbäck, S. (2005). Lack of the Central Nervous System- and Neural Crest-Expressed Forkhead Gene Foxs1 Affects Motor Function and Body Weight. Mol Cell Biol *25*, 5616–5625. https://doi.org/10.1128/MCB.25.13.5616-5625.2005.

47. Sato, Y., Baba, T., Zubair, M., Miyabayashi, K., Toyama, Y., Maekawa, M., Owaki, A., Mizusaki, H., Sawamura, T., Toshimori, K., et al. (2008). Importance of forkhead transcription factor Fkhl18 for development of testicular vasculature. Molecular Reproduction and Development *75*, 1361–1371. https://doi.org/10.1002/mrd.20888.

48. Bates, E.A., Kipp, Z.A., Lee, W.-H., Martinez, G.J., Weaver, L., Becker, K.N., Pauss, S.N., Creeden, J.F., Anspach, G.B., Helsley, R.N., et al. (2024). FOXS1 is increased in liver fibrosis and regulates TGFβ responsiveness and proliferation pathways in human hepatic stellate cells. Journal of Biological Chemistry *300*. https://doi.org/10.1016/j.jbc.2024.105691.

49. Keenan, A.B., Torre, D., Lachmann, A., Leong, A.K., Wojciechowicz, M.L., Utti, V., Jagodnik, K.M., Kropiwnicki, E., Wang, Z., and Ma'ayan, A. (2019). ChEA3: transcription factor enrichment analysis by orthogonal omics integration. Nucleic Acids Res *47*, W212–W224. https://doi.org/10.1093/nar/gkz446.

50. Liu, H., Kennard, S., and Lilly, B. (2009). NOTCH3 Expression Is Induced in Mural Cells Through an Autoregulatory Loop That Requires Endothelial-Expressed JAGGED1. Circulation Research *104*, 466–475. https://doi.org/10.1161/CIRCRESAHA.108.184846.

51. Meng, H., Zhang, X., Hankenson, K.D., and Wang, M.M. (2009). Thrombospondin 2 Potentiates Notch3/Jagged1 Signaling. J Biol Chem *284*, 7866–7874. https://doi.org/10.1074/jbc.M803650200.

52. Mao, C., Ma, Z., Jia, Y., Li, W., Xie, N., Zhao, G., Ma, B., Yu, F., Sun, J., Zhou, Y., et al. (2021). Nidogen-2 Maintains the Contractile Phenotype of Vascular Smooth Muscle Cells and Prevents Neointima Formation via Bridging Jagged1-Notch3 Signaling. Circulation *144*, 1244–1261. https://doi.org/10.1161/CIRCULATIONAHA.120.053361.

53. Liu, Z., Chen, S., Boyle, S., Zhu, Y., Zhang, A., Piwnica-Worms, D.R., Ilagan, M.X.G., and Kopan, R. (2013). The extracellular domain of Notch2 increases its cell-surface abundance and ligand responsiveness during kidney development. Dev Cell *25*, 585–598. https://doi.org/10.1016/j.devcel.2013.05.022.

54. Xu, X., Choi, S.H., Hu, T., Tiyanont, K., Habets, R., Groot, A.J., Vooijs, M., Aster, J.C., Chopra, R., Fryer, C., et al. (2015). Insights into Autoregulation of Notch3 from Structural and Functional Studies of Its Negative Regulatory Region. Structure *23*, 1227–1235. https://doi.org/10.1016/j.str.2015.05.001.

55. Groot, A.J., Habets, R., Yahyanejad, S., Hodin, C.M., Reiss, K., Saftig, P., Theys, J., and Vooijs, M. (2014). Regulated Proteolysis of NOTCH2 and NOTCH3 Receptors by ADAM10 and Presenilins. Mol Cell Biol *34*, 2822–2832. https://doi.org/10.1128/MCB.00206-14.

56. Habets, R.A.J., Groot, A.J., Yahyanejad, S., Tiyanont, K., Blacklow, S.C., and Vooijs, M. (2015). Human NOTCH2 Is Resistant to Ligand-independent Activation by Metalloprotease Adam17. J Biol Chem *290*, 14705–14716. https://doi.org/10.1074/jbc.M115.643676.

57. Landor, S.K.J., Santio, N.M., Eccleshall, W.B., Paramonov, V.M., Gagliani, E.K., Hall, D., Jin, S.-B., Dahlström, K.M., Salminen, T.A., Rivero-Müller, A., et al. (2021). PIM-induced phosphorylation of Notch3 promotes breast cancer tumorigenicity in a CSL-independent fashion. Journal of Biological Chemistry *296*. https://doi.org/10.1016/j.jbc.2021.100593.

58. Liu, Z., Brunskill, E., Varnum-Finney, B., Zhang, C., Zhang, A., Jay, P.Y., Bernstein, I., Morimoto, M., and Kopan, R. (2015). The intracellular domains of Notch1 and Notch2 are functionally equivalent during development and carcinogenesis. Development *142*, 2452–2463. https://doi.org/10.1242/dev.125492.

59. He, L., Vanlandewijck, M., Mäe, M.A., Andrae, J., Ando, K., Del Gaudio, F., Nahar, K., Lebouvier, T., Laviña, B., Gouveia, L., et al. (2018). Single-cell RNA sequencing of mouse brain and lung vascular and vessel-associated cell types. Sci Data *5*, 180160. https://doi.org/10.1038/sdata.2018.160.

60. Vanlandewijck, M., He, L., Mäe, M.A., Andrae, J., Ando, K., Del Gaudio, F., Nahar, K., Lebouvier, T., Laviña, B., Gouveia, L., et al. (2018). A molecular atlas of cell types and zonation in the brain vasculature. Nature *554*, 475–480. https://doi.org/10.1038/nature25739.

61. van Engeland, N.C.A., Suarez Rodriguez, F., Rivero-Müller, A., Ristori, T., Duran, C.L., Stassen, O.M.J.A., Antfolk, D., Driessen, R.C.H., Ruohonen, S., Ruohonen, S.T., et al. (2019). Vimentin regulates Notch signaling strength and arterial remodeling in response to hemodynamic stress. Sci Rep *9*, 12415. https://doi.org/10.1038/s41598-019-48218-w.

62. van Asten, J.G.M., Ristori, T., Nolan, D.R., Lally, C., Baaijens, F.P.T., Sahlgren, C.M., and Loerakker, S. (2022). Computational analysis of the role of mechanosensitive Notch signaling in arterial adaptation to hypertension. Journal of the Mechanical Behavior of Biomedical Materials *133*, 105325. https://doi.org/10.1016/j.jmbbm.2022.105325.

63. van Asten, J.G.M., Latorre, M., Karakaya, C., Baaijens, F.P.T., Sahlgren, C.M., Ristori, T., Humphrey, J.D., and Loerakker, S. (2023). A multiscale computational model of arterial growth and remodeling including Notch signaling. Biomech Model Mechanobiol *22*, 1569–1588. https://doi.org/10.1007/s10237-023-01697-3.

64. Briot, A., Jaroszewicz, A., Warren, C.M., Lu, J., Touma, M., Rudat, C., Hofmann, J.J., Airik, R., Weinmaster, G., Lyons, K., et al. (2014). Repression of Sox9 by Jag1 Is Continuously Required to Suppress the Default Chondrogenic Fate of Vascular Smooth

Muscle Cells. Developmental Cell *31*, 707–721. https://doi.org/10.1016/j.devcel.2014.11.023.

65. High, F.A., Lu, M.M., Pear, W.S., Loomes, K.M., Kaestner, K.H., and Epstein, J.A. (2008). Endothelial expression of the Notch ligand Jagged1 is required for vascular smooth muscle development. Proc Natl Acad Sci U S A *105*, 1955–1959. https://doi.org/10.1073/pnas.0709663105.

66. Travisano, S.I., Oliveira, V.L., Prados, B., Grego-Bessa, J., Piñeiro-Sabarís, R., Bou, V., Gómez, M.J., Sánchez-Cabo, F., MacGrogan, D., and De La Pompa, J.L. (2019). Coronary arterial development is regulated by a Dll4-Jag1-EphrinB2 signaling cascade. eLife *8*, e49977. https://doi.org/10.7554/eLife.49977.

67. Feng, X., Krebs, L.T., and Gridley, T. (2010). Patent ductus arteriosus in mice with smooth muscle-specific Jag1 deletion. Development *137*, 4191–4199. https://doi.org/10.1242/dev.052043.

68. Hogan, B.M., and Schulte-Merker, S. (2017). How to Plumb a Pisces: Understanding Vascular Development and Disease Using Zebrafish Embryos. Developmental Cell *42*, 567–583. https://doi.org/10.1016/j.devcel.2017.08.015.

69. Lange, M., Granados, A., VijayKumar, S., Bragantini, J., Ancheta, S., Kim, Y.-J., Santhosh, S., Borja, M., Kobayashi, H., McGeever, E., et al. (2024). A multimodal zebrafish developmental atlas reveals the state-transition dynamics of late-vertebrate pluripotent axial progenitors. Cell *187*, 6742-6759.e17. https://doi.org/10.1016/j.cell.2024.09.047.

70. Ando, K., Ishii, T., and Fukuhara, S. (2021). Zebrafish Vascular Mural Cell Biology: Recent Advances, Development, and Functions. Life *11*, 1041. https://doi.org/10.3390/life11101041.

71. Hao, Y., Hao, S., Andersen-Nissen, E., Mauck, W.M., Zheng, S., Butler, A., Lee, M.J., Wilk, A.J., Darby, C., Zager, M., et al. (2021). Integrated analysis of multimodal single-cell data. Cell *184*, 3573-3587.e29. https://doi.org/10.1016/j.cell.2021.04.048.

72. Whitesell, T.R., Chrystal, P.W., Ryu, J.-R., Munsie, N., Grosse, A., French, C.R., Workentine, M.L., Li, R., Zhu, L.J., Waskiewicz, A., et al. (2019). *foxc1* is required for embryonic head vascular smooth muscle differentiation in zebrafish. Developmental Biology *453*, 34–47. https://doi.org/10.1016/j.ydbio.2019.06.005.

73. Ando, K., Tong, L., Peng, D., Vázquez-Liébanas, E., Chiyoda, H., He, L., Liu, J., Kawakami, K., Mochizuki, N., Fukuhara, S., et al. (2022). KCNJ8/ABCC9-containing K-ATP channel modulates brain vascular smooth muscle development and neurovascular coupling. Developmental Cell *57*, 1383-1399.e7. https://doi.org/10.1016/j.devcel.2022.04.019.

74. Hombría, J.C.-G., García-Ferrés, M., and Sánchez-Higueras, C. (2021). Anterior Hox Genes and the Process of Cephalization. Front. Cell Dev. Biol. *9*. https://doi.org/10.3389/fcell.2021.718175.

75. Choy, L., Hagenbeek, T.J., Solon, M., French, D., Finkle, D., Shelton, A., Venook, R., Brauer, M.J., and Siebel, C.W. (2017). Constitutive NOTCH3 Signaling Promotes the Growth of Basal Breast Cancers. Cancer Research *77*, 1439–1452. https://doi.org/10.1158/0008-5472.CAN-16-1022.

76. Peterson, S.M., Turner, J.E., Harrington, A., Davis-Knowlton, J., Lindner, V., Gridley, T., Vary, C.P.H., and Liaw, L. (2018). Notch2 and Proteomic Signatures in Mouse Neointimal Lesion Formation. Arteriosclerosis, Thrombosis, and Vascular Biology *38*, 1576–1593. https://doi.org/10.1161/ATVBAHA.118.311092.

77. Davis-Knowlton, J., Turner, J.E., Harrington, A., and Liaw, L. (2022). Smooth Muscle Cell Notch2 Is Not Required for Atherosclerotic Plaque Formation in ApoE Null Mice. Journal of Vascular Research *59*, 261–274. https://doi.org/10.1159/000525258.

78. Machuca-Parra, A.I., Bigger-Allen, A.A., Sanchez, A.V., Boutabla, A., Cardona-Vélez, J., Amarnani, D., Saint-Geniez, M., Siebel, C.W., Kim, L.A., D'Amore, P.A., et al. (2017). Therapeutic antibody targeting of Notch3 signaling prevents mural cell loss in CADASIL. Journal of Experimental Medicine *214*, 2271–2282. https://doi.org/10.1084/jem.20161715.

79. Joutel, A., Vahedi, K., Corpechot, C., Troesch, A., Chabriat, H., Vayssière, C., Cruaud, C., Maciazek, J., Weissenbach, J., Bousser, M.-G., et al. (1997). Strong clustering and stereotyped nature of Notch3 mutations in CADASIL patients. The Lancet *350*, 1511–1515. https://doi.org/10.1016/S0140-6736(97)08083-5.

80. Joutel, A., Andreux, F., Gaulis, S., Domenga, V., Cecillon, M., Battail, N., Piga, N., Chapon, F., Godfrain, C., and Tournier-Lasserve, E. (2000). The ectodomain of the Notch3 receptor accumulates within the cerebrovasculature of CADASIL patients. J Clin Invest *105*, 597–605. https://doi.org/10.1172/JCI8047.

81. Monet-Leprêtre, M., Haddad, I., Baron-Menguy, C., Fouillot-Panchal, M., Riani, M., Domenga-Denier, V., Dussaule, C., Cognat, E., Vinh, J., and Joutel, A. (2013). Abnormal recruitment of extracellular matrix proteins by excess Notch3ECD: a new pathomechanism in CADASIL. Brain *136*, 1830–1845. https://doi.org/10.1093/brain/awt092.

82. Andersson, E.R., Chivukula, I.V., Hankeova, S., Sjöqvist, M., Tsoi, Y.L., Ramsköld, D., Masek, J., Elmansuri, A., Hoogendoorn, A., Vazquez, E., et al. (2018). Mouse Model of Alagille Syndrome and Mechanisms of Jagged1 Missense Mutations. Gastroenterology *154*, 1080–1095. https://doi.org/10.1053/j.gastro.2017.11.002.

83. Hankeova, S., Van Hul, N., Laznovsky, J., Verboven, E., Mangold, K., Hensens, N., Adori, C., Verhoef, E., Zikmund, T., Dawit, F., et al. (2022). Sex differences and risk factors for bleeding in Alagille syndrome. EMBO Mol Med *14*, e15809. https://doi.org/10.15252/emmm.202215809.

84. Dupré, N., Gueniot, F., Domenga-Denier, V., Dubosclard, V., Nilles, C., Hill-Eubanks, D., Morgenthaler-Roth, C., Nelson, M.T., Keime, C., Danglot, L., et al. (2024). Protein aggregates containing wild-type and mutant NOTCH3 are major drivers of arterial pathology in CADASIL. J Clin Invest *134*. https://doi.org/10.1172/JCI175789.

85. Karakaya, C., van Turnhout, M.C., Visser, V.L., Ristori, T., Bouten, C.V.C., Sahlgren, C.M., and Loerakker, S. (2022). Notch signaling regulates strain-mediated phenotypic switching of vascular smooth muscle cells. Front. Cell Dev. Biol. *10*. https://doi.org/10.3389/fcell.2022.910503.

86. Ando, K., Wang, W., Peng, D., Chiba, A., Lagendijk, A.K., Barske, L., Crump, J.G., Stainier, D.Y.R., Lendahl, U., Koltowska, K., et al. (2019). Peri-arterial specification of vascular mural cells from naïve mesenchyme requires Notch signaling. Development *146*, dev165589. https://doi.org/10.1242/dev.165589.

87. Nandagopal, N., Santat, L.A., LeBon, L., Sprinzak, D., Bronner, M.E., and Elowitz, M.B. (2018). Dynamic Ligand Discrimination in the Notch Signaling Pathway. Cell *172*, 869-880.e19. https://doi.org/10.1016/j.cell.2018.01.002.

88. Bernard, F., Krejci, A., Housden, B., Adryan, B., and Bray, S.J. (2010). Specificity of Notch pathway activation: Twist controls the transcriptional output in adult muscle progenitors. Development *137*, 2633–2642. https://doi.org/10.1242/dev.053181.

89. O'Brien, L.L., Grimaldi, M., Kostun, Z., Wingert, R.A., Selleck, R., and Davidson, A.J. (2011). Wt1a, Foxc1a, and the Notch mediator Rbpj physically interact and regulate the formation of podocytes in zebrafish. Developmental Biology *358*, 318–330. https://doi.org/10.1016/j.ydbio.2011.08.005.

90. Sahlgren, C., Gustafsson, M.V., Jin, S., Poellinger, L., and Lendahl, U. (2008). Notch signaling mediates hypoxia-induced tumor cell migration and invasion. Proceedings of the National Academy of Sciences *105*, 6392–6397. https://doi.org/10.1073/pnas.0802047105.

91. Antfolk, D., Sjöqvist, M., Cheng, F., Isoniemi, K., Duran, C.L., Rivero-Muller, A., Antila, C., Niemi, R., Landor, S., Bouten, C.V.C., et al. (2017). Selective regulation of Notch ligands during angiogenesis is mediated by vimentin. Proceedings of the National Academy of Sciences *114*, E4574–E4581. https://doi.org/10.1073/pnas.1703057114.

92. Sur, A., Wang, Y., Capar, P., Margolin, G., Prochaska, M.K., and Farrell, J.A. (2023). Single-cell analysis of shared signatures and transcriptional diversity during zebrafish

885 development. Developmental Cell *58*, 3028-3047.e12.
886 https://doi.org/10.1016/j.devcel.2023.11.001.

887 93. Choi, H.M.T., Schwarzkopf, M., Fornace, M.E., Acharya, A., Artavanis, G., Stegmaier, J.,
888 Cunha, A., and Pierce, N.A. (2018). Third-generation in situ hybridization chain reaction:
889 multiplexed, quantitative, sensitive, versatile, robust. Development *145*, dev165753.
890 https://doi.org/10.1242/dev.165753.

891 94. Schindelin, J., Arganda-Carreras, I., Frise, E., Kaynig, V., Longair, M., Pietzsch, T.,
892 Preibisch, S., Rueden, C., Saalfeld, S., Schmid, B., et al. (2012). Fiji: an open-source
893 platform for biological-image analysis. Nat Methods *9*, 676–682.
894 https://doi.org/10.1038/nmeth.2019.

895 95. Sprinzak, D., Lakhanpal, A., LeBon, L., Santat, L.A., Fontes, M.E., Anderson, G.A.,
896 Garcia-Ojalvo, J., and Elowitz, M.B. (2010). Cis-interactions between Notch and Delta
897 generate mutually exclusive signalling states. Nature *465*, 86–90.
898 https://doi.org/10.1038/nature08959.

899 96. Boareto, M., Jolly, M.K., Lu, M., Onuchic, J.N., Clementi, C., and Ben-Jacob, E. (2015).
900 Jagged–Delta asymmetry in Notch signaling can give rise to a Sender/Receiver hybrid
901 phenotype. Proc. Natl. Acad. Sci. U.S.A. *112*.
902 https://doi.org/10.1073/pnas.1416287112.

903 97. Konishi, T., Ghosh, S.K.B., Sato, Y., Kawakami, R., Kawai, K., Vozenilek, A.E., Xu, W.,
904 Bellissard, A., Giasolli, R., Chahal, D., et al. (2023). The histological analysis of the
905 coronary medial thickness: Implications for percutaneous coronary intervention. PLOS
906 ONE *18*, e0283840. https://doi.org/10.1371/journal.pone.0283840.

907 98. Ando, K., Fukuhara, S., Izumi, N., Nakajima, H., Fukui, H., Kelsh, R.N., and Mochizuki,
908 N. (2016). Clarification of mural cell coverage of vascular endothelial cells by live
909 imaging of zebrafish. Development *143*, 1328–1339.
910 https://doi.org/10.1242/dev.132654.

911

912 **Methods**

913 Cell Culture and Maintenance

914 Human aortic smooth muscle cells (SMCs) were purchased from Lonza (Cat. #CC-2571) and
915 American Type Culture Collection (ATCC Cat. #PCS-100-012) in passages 3 or 2 (See the
916 Resources Table for details). The cells were grown in Smooth Muscle Basal Medium containing
917 SmGM®-2 SingleQuots supplements (Lonza Cat. #CC-3182) until passage 4-6 and used within
918 15 population doublings. Human umbilical vein endothelial cells (HUVECs) were bought from
919 PromoCell (Cat. #C-12200) at passage 1 and grown in Endothelial Cell Growth Medium 2
920 (PromoCell Cat.#C-22011) until passage number 4. Human embryonic kidney cell line HEK 293T
921 was grown in Dulbecco´s Modified Eagle´s Medium (Merck Cat. #D6429) supplemented with 10%
922 fetal bovine serum (Gibco Cat. #17914671), 2 mM L-glutamine (Merck Cat. #G7513) and 100
923 units/ml penicillin/streptomycin (Merck Cat. #P0781). All cells were maintained at 37°C with 5%
924 CO_2 and kept under 80% confluency at all times unless the experimental setting required
925 otherwise.

926 RNA interference and Plasmids

927 For siRNA transfections, 10^4 SMCs per cm^2 were plated in 6cm culture dishes and grown
928 overnight. The next morning, the cells were transfected with 25nM Dharmacon ON-TARGETplus
929 SMARTPool siRNAs (Horizon Discovery) for the indicated genes or with the same concentration
930 of non-targeting siRNA (Eurofins Genomics) using RNAiMAX lipofectamine (Thermo Fisher
931 Scientific Cat. #13778150). Briefly, the siRNAs and the lipofectamine solutions were separately
932 prepared in Opti-MEM (Gibco Cat. #31985062). The lipofectamine solution was dropwise added
933 to the siRNA solution and mixed gently by flicking the tubes. The solution was then briefly
934 centrifuged and left to incubate for 15 min at RT. The cells were supplied with fresh growth media.
935 The siRNA mix was dropwise added to the culture plate and swirled gently to mix. The cells were
936 then incubated for 24 or 48 hours according to the experimental setting before use. 10

937 For plasmid transfection, HEK 293T cells were grown to 70% confluence in 10 cm culture dishes.
938 The indicated plasmids were transfected using jetOPTIMUS transfection kit (Sartorius Cat.
939 #101000006) at 1µg/ml concentration, according to the supplier´s recommendations. Briefly, the
940 plasmids and the transfection reagent were added to the supplied buffer and mixed using a vortex
941 for 1 second. The tube was centrifuged for 10 s and left to incubate for 10 min. The solution was
942 then dropwise added to the culture plate that was supplied with fresh, warm media. The cells were
943 then incubated overnight before use.

944 Notch trans-activation assays

945 For the Notch activation assays, the recombinant human Jagged1-Fc chimeric ligands (Bio-
946 techne Cat. #1277-JG) were immobilized on the culture plates at 10nM concentration as
947 described previously[90]. Briefly, the culture plates were first treated with 50µg/ml protein G (Thermo
948 Fisher Scientific Cat. #21193) in phosphate-buffered saline (PBS) (Biowest Cat. #L0616)
949 overnight at RT. The next day, the plates were washed three times with PBS and blocked with 1%
950 bovine serum albumin (BSA) (Merck Cat. #A9418) in PBS for 1 hour at RT. Then, the plates were
951 treated with the ligands in PBS with 0.1% BSA overnight at cold or 2 hours at RT. The plates were

952 washed three times with PBS before use. The cells were plated on the immobilized ligands right
953 away. In all experiments, human IgG_1 Fc (Bio-techne Cat. #110-HG) was used as a negative
954 control.

955 For the DAPT washout experiments, the cells were plated on the ligands in media containing
956 10μM DAPT ((2S)- N- [(3,5- Difluoro phenyl)acetyl]- L- alanyl- 2- phenyl]glycine 1,1- dimethyl ethyl
957 ester) (Bio-Techne Cat. #2634-10) or DMSO (dimethyl sulfoxide) (Merck Cat. #D2650) as the
958 vector control where appropriate and let recover for 24 hours. The next day, the DAPT was
959 removed by replacing the media with fresh, warm media, and the cells were incubated for the
960 indicated time until use.

961 For the TGFβR inhibition experiments, the cells were plated on the ligands with media containing
962 10μM SB-431542 (MedChemExpress, Cat. #HY-10431), 10μM DAPT, or DMSO and incubated
963 for either 24h hours for qPCR or 72 hours for immunoblotting. The cells were supplied with media
964 containing fresh dilutions of the inhibitors every 24 hours until lysis.

965 Ligand binding assays and Flow Cytometry

966 The live Notch staining assay was done as described previously[91] with few adjustments. 10^4
967 SMCs per cm^2 transfected with siRNAs against Notch2 and Notch3 were plated 24 hours post-
968 transfection and left to incubate for another 24 hours. The next day the cells were blocked with
969 sterile-filtered SmGM®-2 containing 1% BSA and 10% goat serum (Biowest Cat. #S2000) for 45
970 min at 37°C with 5% CO_2. 50nM Jagged1-Fc was conjugated with anti-human Alexa fluor 488
971 antibodies (Thermo Fisher Scientific Cat. #21091) at 1:200 dilution in PBS for 1 hour at cold. The
972 ligand dilution was added directly to the blocking media at a 1:5 ratio to achieve a final ligand
973 concentration of 10nM and incubated for 2 hours at 37°C with 5% CO_2. The cells were either used
974 for microscopy following fixation or live for flow cytometry. For microscopy, the cells were washed
975 three times with HEPES-buffered saline solution (Lonza Cat. #CC-5024), fixed with 4% PFA in
976 PBS for 10 min at RT, and mounted using Vectashield with DAPI (4',6-diamidino-2-phenylindole,
977 dihydrochloride) (Vector Laboratories Cat. #H-1000). The samples were imaged using the 3i CSU-
978 W1 spinning disc confocal microscope.

979 For flow cytometry, the cells were washed three times with HEPES buffered saline solution and
980 detached using ReagentPack™ subculture reagents (Lonza Cat. #CC50-34) at RT. The cells were
981 immediately taken on ice and collected into 1.5 ml centrifuge tubes. The cells were washed with
982 ice-cold HEPES buffered saline solution three times by centrifuging for 3 min at 500 RCF, 4°C,
983 and resuspending in fresh buffer. The cells were analyzed with BD LSR Fortessa flow cytometer
984 using 488 nm excitation wavelength. The data were analyzed using the FlowJo software (v.10)
985 and presented as mean fluorescence intensity.

986 Notch reporter assay

987 The luciferase assay was done as described previously[57]. HEK 293T cells were transfected with
988 0.1μg 12xCSL-Luciferase (RBPJκ) and 0.1μg β-galactosidase along with increasing
989 concentrations (0-1.8μg) of Flag-tagged Notch2 or Notch3 intracellular domain (NICD2 and
990 NICD3) constructs. Each transfection was completed to 2μg using the plasmid, only bearing Flag.
991 An extra set of cells was prepared in parallel to assess NICD abundance by immunoblotting. The

992 next day, the cells were lysed in passive lysis buffer (Promega Cat. #E1941). The luciferase
993 activity was measured using VivoGlo™ luciferin (Promega Cat. #P1041) and normalized to β-
994 galactosidase activity.

995 Spheroid formation

996 $8x10^3$ SMCs were grown in Nuncleon™ Sphera™ low adhesion plates (Thermo Fisher Scientific
997 Cat. #174929) for 72 hours in SMGM-2 media to form mono-culture SMC spheroids. For the co-
998 culture spheroids, SMCs were first grown for 48 hours alone and then for 24 hours with $3x10^3$
999 HUVECs. The spheroids were washed once with PBS, then fixed and permeabilized in PBS
1000 containing 4% paraformaldehyde and 1% Triton X-100 (VWR, Cat. #M143) overnight at cold. They
1001 were washed three times for 15 min each in PBS with 0.1% Triton X-100 and incubated with 1:100
1002 mouse CD31 (Thermo Fisher Scientific Cat. #37-0700) and 1:100 rabbit Jagged1 (Cell Signaling
1003 Cat. #2620) primary antibodies overnight at cold. The spheroids were washed three times and
1004 incubated with 1:400 dilutions of the anti-rabbit Alexa fluor 488 (Thermo Fisher Scientific Cat. #A-
1005 11034) and anti-mouse Alexa fluor 555 antibodies (Thermo Fisher Scientific Cat. #A-21422). After
1006 three more washes, the spheroids were mounted in glycerol (Merck Cat. #G5516). The samples
1007 were imaged using the 3i CSU-W1 spinning disc confocal microscope. The mean Jagged1 signal
1008 in confocal slices from the middle of the spheroids was quantified using Fiji ImageJ and
1009 normalized by subtracting the intensity of the control samples without primary antibodies. At least
1010 four spheroids were analyzed per group for each independent experiment. The normalized signal
1011 was presented as a fold change.

1012 RNA isolation, qPCR, and Next Generation Sequencing

1013 RNA was isolated from SMCs using NucleoSpin RNA (Macharey-Nagel Cat. #740955) according
1014 to the supplier´s protocol. The RNA concentration and quality were checked using Nanodrop ND-
1015 2000, Thermore Fisher Scientific. The resulting RNA was used for cDNA library preparation using
1016 the SensiFAST™ cDNA synthesis kit (Bioline Cat. #BIO-65054). The quantitative polymerase
1017 chain reaction (qPCR) using 5x HOT FIREPol EvaGreen qPCR Mix Plus reagent (Labnet Cat.
1018 #08-24-00001-10) according to the supplier´s protocol using Quanstudio Real-Time PCR system,
1019 Thermo Fisher Scientific. The qPCR primers for the indicated genes were ordered from TAG
1020 Copenhagen (See the Resources Table for the primer sequences). For all primer pairs, a cDNA
1021 dilution series, prepared from a cocktail of samples from the same experiment, was included in
1022 the same qPCR run to calculate a standard curve. The standard curve was used to calculate the
1023 relative mRNA expression.

1024 The bulk RNA sequencing (RNAseq) was performed in the Finnish Cultural Genomics Center,
1025 University of Turku. For each sample, a starting quantity of 100 ng RNA was processed. Sample
1026 quality was ensured using Agilent BioAnalyzer 2100. Sample concentration was measured with
1027 Qubit®/Quant-IT® Fluorometric Quantitation, Life Science Technologies. The library preparation
1028 was done according to the guidelines from Illumina Stranded mRNA Preparation, Illumina
1029 (1000000124518) using Illumina Stranded mRNA Preparation, Ligation, Kit (Illumina). The
1030 average fragment size was 335 bp. The base calling was done using the bcl2fastq2 software on
1031 NovaSeq 6000. Sequencing was done using Illumina NovaSeq 6000 S1 v1.5, with paired-end
1032 sequencing and 2 x 50 bp read length.

1033 The read quality was checked with FastQC (v.0.11.8). The reads were aligned against the hg38
1034 human genome (Illumina iGenome: https://support.illumina.com/sequencing/sequencing
1035 software/igenome.html (UCSC)) and annotated using the Rsubread package (v.2.6.4) in
1036 Bioconductor (v.3.13), R (v.4.1.0). The gene ids were matched to the gene symbols using the
1037 org.Hs.eg.db package (v.3.13.0). Normalization was done with edgeR (v.3.34.1) to produce
1038 counts per million (CPM) and reads per kilo read per million (RPKM) for each gene. Pairwise
1039 comparisons between groups were performed using ROTS (v.1.20.0) on log2(1+CPM). This part
1040 of the sequencing data analysis was done in the Medical Bioinformatics Center, University of
1041 Turku.

1042 For biological interpretation, z scores were calculated based on log_2(1+CPM) across all groups
1043 from each time point separately. The genes were then clustered using Ward´s method and used
1044 to build a heatmap using the pheatmap package (v.1.0.12). Gene ontology analysis for biological
1045 processes on each cluster was performed with the clusterprofiler package(v.4.14.4).

1046 Immunoblotting

1047 All samples were lysed in 3x Laemmli buffer (0.1875 M Tris, 0.21 M SDS, 30% glycerol,
1048 bromphenol blue) containing 3% 2-mercaptoethanol (Merck, Cat. #444233) on ice, scraped into
1049 1.5 ml centrifuge tubes, and boiled at 95°C for 10 minutes. The lysates were separated by SDS-
1050 PAGE and transferred onto nitrocellulose membranes (Cytiva, Cat. #15220033). The membranes
1051 were checked for loading using Revert™ 700 Total Protein Stain (LI-COR Cat. #926-11016),
1052 blocked with 1% w/v milk in PBS with 0.1% Tween 20 (VWR Cat. #M147) for 30 min and probed
1053 with the antibodies indicated below. The bands were visualized using SuperSignal™ West
1054 Picoplus chemiluminescent substrate kit (Thermo Fisher Scientific Cat. #34580) and imaged with
1055 iBright FL1000, Thermo Fisher Scientific. The bands were analyzed using the ImageStudio Lite
1056 software (v.6.0), LI-COR. Unless stated otherwise, all bands were normalized to total protein stain.
1057 The primary antibodies used: Notch2 1:1000 (Cell Signaling Cat. #5732), Notch3 1:1000 (Cell
1058 Signaling Cat. #5276), Jagged1 1:1000 (Cell Signaling Cat. #2620), α-SMA 1:1000(Cell Signaling
1059 Cat. #19245), Pdgfrβ 1:1000 (Cell Signaling Cat. #3169), β-tubulin 1:1000 (Cell Signaling Cat.
1060 #86298), His-Tag 1:1000 (Cell Signaling Cat. #2365), M2-Flag 1:1000 (Merck, Cat. #F1804),
1061 smad2/3 1:200 (Santa Cruz Cat. #sc-133098), and phospho-smad2 1:1000 (Cell Signaling Cat.
1062 #3108), β-actin 1:10000 (Merck Cat. #A1978). The horse radish peroxidase-conjugated
1063 secondary antibodies used: anti-rabbit 1:10000 (Vector Laboratories, #PI-1000), anti-mouse
1064 1:10000 (Vector Laboratories, #PI-2000), Veriblot for IP detection 1:500 (Abcam, Cat.
1065 #ab131366).

1066 Immunoprecipitation

1067 HEK 293T cells expressing Flag-NICD and 6xHis-RBPJκ were lysed in RIPA buffer (50 mM Tris-
1068 HCl pH = 8.0, 1% Triton X-100, 1% sodium deoxycholate acid, 0.1% SDS, 1 mM Na4VO3, 50 mM
1069 NaCl, 10 mM NaF, and 1 mM EDTA) containing 1x cOmplete™ protease inhibitors (Roche, Cat.
1070 #05892970001) on ice for 10 min. The lysates were scraped into 1.5 ml Eppendorf tubes and
1071 centrifuged for 15 min at 14 000 RCF, 4°C. A total of 1.5 mg protein was immunoprecipitated with
1072 40µl of anti-Flag affinity agarose beads (Merck, Cat. #A2220) on rotation for 1 hour at 4°C. The

1073 beads were washed with the lysis buffer three times and boiled in 3x Laemmli buffer for 10 minutes
1074 at 95°C.

1075 Re-analysis of single-cell RNAseq data

1076 For the vascular cells from different organs, previously published normalized datasets from the
1077 Betsholtz lab[59,60,36] were downloaded from Gene Expression Omnibus under the accession codes
1078 GSE98816 (brain), GSE20100 (lung), GSE210087 (heart), GSE210013 (colon), and GSE21000
1079 (aorta). The expression matrices were read using the general Seurat scRNAseq analysis pipeline
1080 (v.4.4). For the datasets except the brain data, the ENSEMBL IDs were converted to gene symbols
1081 using Org.Mm.eg.db (v.3.20.0) and AnnotationDbi (v.1.68.0), and the duplicates and the entries
1082 without symbols were removed. Each dataset was then processed according to the Seurat
1083 workflow. Gene expression was normalized to 10000 counts and log-transformed. The clusters
1084 were created using the FindClusters function with the resolution set to 0.5 for the aorta dataset
1085 and 1 for the rest. The UMAP was calculated for brain, lung, heart, colon, and aorta datasets from
1086 the top 20, 25, 20, 20, and top 15 PCs, respectively. The cluster annotations were partly adapted
1087 from Muhl et al.[36]. SMCs, Acta2, Myh11, Tagln, and Cspg4 were used as SMC markers, while
1088 Chrdl1, Hhip, Shisa3, Ccl19, Chrm2, Bdkrb2, and Abcc9 were used to filter out the non-arterial
1089 SMCs and pericytes. For the heart dataset, the cluster positive for Itgbl1 was annotated as aortic
1090 SMCs proximal to the heart. The clusters positive for Pecam1 and Kdr and negative for Prox1
1091 were annotated as vascular endothelial cells. The clusters were extracted from the count matrices
1092 using the annotated cell IDs from the Seurat objects. The SMC and the EC data were processed
1093 separately. The datasets were filtered only to include the common genes among the different
1094 organs. The extracted matrices were re-normalized individually using “RC” transformation. No
1095 data integration or batch correction were deemed necessary as the datasets were used only for
1096 the comparison of single genes.

1097 The processed mesoderm dataset was downloaded from Zebrahub. The expression matrix and
1098 the metadata files were extracted using the Scanpy tool in Python and used to create a Seurat
1099 object. This dataset was already log-normalized and scaled and did not contain the raw counts.
1100 Hence, the PCA analysis was done manually using the first 50 components. The clusters were
1101 found using the resolution set to 0.5, and the UMAPs were found using the top 5 PCs. Markers
1102 for all clusters were found using the FindAllMarkers command. The markers for non-vascular
1103 associated SMC markers were checked using the Daniocell[92] single-cell RNAseq database.
1104 Based on this, the clusters highly expressing, desmb, nkx2.3, and nrg1 were used to filter out the
1105 non-vascular SMCs (Figure S4). The clusters from embryos younger than 3 dpf were left out of
1106 the analysis. The remaining SMC clusters were annotated based on larval day and notch3
1107 expression. The VlnPlot function was used to plot the normalized counts based on the new
1108 annotations.

1109 Zebrafish lines and reporter assays

1110 All zebrafish work was carried out in the Zebrafish Core Facility at Turku Bioscience Center under
1111 license ESAVI/31414/2020 and ESAVI/44584/2023 granted by the Regional Administration Office
1112 of Southern Finland. The offspring of transgenic zebrafish heterozygous for tagln (tagln:GFP) or
1113 kdrl (kdrl:mcherry) were injected with 10ng control, Notch2, or Notch3 morpholinos (Gene Tools

1114 Store) before the 8-cell stage. Embryos were kept in E3 media (5 mM NaCl, 0.17 mM KCl, 0.33
1115 mM $CaCl_2$, 0.33 mM $MgSO_4$) supplemented with 30 mg/ml of 1-phenyl 2-thiourea (PTU) (Merck,
1116 Cat. #P7629) at 28.5°C. At 4 dpf, the larvae positive for both reporters were mounted dorsally in
1117 2% agarose molds, immobilized with 1% agarose, and imaged in the same media containing 160
1118 mg/ml tricaine (Merck, Cat. #E10521) using MSquared Aurora light sheet microscope with 0.4 µm
1119 slice thickness. The stacks were stitched using the Zeiss Arivis Vision 4D software (v.3.5.) and
1120 analyzed using the Oxford Instruments Imaris image analysis software (v.10.2.0). Briefly, the
1121 endothelium marked with kdrl and the tagln+ objects were surface-rendered following pseudo-flat
1122 field correction for uneven illumination. The tagln+ objects that were at least in 5µm proximity of
1123 the endothelium were considered vascular-associated. In the hind/midbrain region, the objects
1124 that were deemed artifacts of the tagln+ tip of the notochord were manually chosen and left out
1125 of the analysis. The number of tagln+ objects in the dorsal aorta was normalized to the length of
1126 the measured region and presented in arbitrary units.

1127 *In situ* hybridization chain reaction (HCR)

1128 3 dpf transgenic larvae expressing a pdgfrb reporter (UAS:EGFP, pdgfrb:GAL4FF) were
1129 euthanized in E3 media with tricaine at cold for 1h and fixed in 4% PFA overnight at cold. After
1130 five washes with PBS, the embryos were dehydrated and permeabilized in methanol at RT four
1131 times for 10 min and once for 50 min and rehydrated with four gradually decreasing concentrations
1132 of MeOH in PBS with 0.1% Tween 20 (PBST) for 5 min each. The larvae were treated with
1133 RNAScope™ Protease Plus (Biotechne, Cat. #322331) for 30 min at RT and quickly washed
1134 twice with PBS. The larvae were post-fixed in 4% PFA at RT for 20 min, washed five times with
1135 PBS for 5 min each, and used for HCR™ Gold RNA (Molecular Instruments) *in situ* hybridization
1136 reaction according to the suppliers' protocol, adapted from Choi et al.[93]. The notch2 and the
1137 notch3 probes were visualized using x2-546 and x1-647 hairpin pairs, respectively. The fish were
1138 mounted ventrally directly on 35 mm glass-bottom confocal dishes (VWR, Cat. #75856) in 1%
1139 agarose (w/v) and imaged by taking z-stacks using the 3i CSU-W1 spinning disc confocal
1140 microscope with the 25x/0.8 Imm Korr DIC objective with silicone oil (Zeiss). The images were
1141 cropped to zoom in on the arterial regions using Fiji ImageJ[94] (v.2.16.0).

1142 Statistical analysis

1143 All statistical analyses were done using GraphPad Prism (v.10). For single factor experiments,
1144 the normal distribution of the data and the residuals were checked, and one-way ANOVA followed
1145 by Tukey´s, Dunnet´s, or Sidak´s post-hoc tests were used. For two-factor experiments, two-way
1146 ANOVA followed by Tukey´s, Dunnet´s, or Sidak´s post-hoc tests were used. The data were
1147 plotted using GraphPad Prism (v.10) or ggplot2 in R. The p values smaller than 0.1 were denoted
1148 on the plots. The details for the statistical methods and the experimental replicates are given in
1149 the figure legends.

1150 Computational Model for Extrinsic Ligand Induction

1151 To simulate the experimental scenarios of Notch signaling in a cluster of SMCs, we extended a
1152 previous computational framework of Notch signaling (AB model developed by Loerakker et al.[13]
1153 and Ristori et al.[14], based on Sprinzak et al.[95] and Boareto et al.[96]) in a periodic one-dimensional
1154 array of SMCs, by incorporating the separate effects of Notch2-Jagged1 and Notch3-Jagged1

binding on the signaling dynamics. The levels of key proteins (Notch2, Notch3 Jagged, NICD) were predicted for each cell, with interactions allowed between neighboring cells on either side. The temporal changes in Notch (N), Jagged (J), and NICD (I) concentrations within cell i at time t were modeled using the following differential equations:

$$\frac{d\ \ {}^{i}_{3}}{dt} = N_3^{pr} H\left(I_{N2}^{i},\ I_{0,N2}, n_{N2}, \lambda_{N2}\right) H\left(I_{N3}^{i},\ I_{0,N3}, n_{N3}, \lambda_{N3}\right) - N_3^i\ (k_c J^i + k_t J_{ext}^i) - \gamma N_3^i \quad (1)$$

$$\frac{d\ \ {}^{i}_{2}}{dt} = N_2^{pr} - N_2^i\ (k_c J^i + k_t J_{ext}^i) - \gamma N_2^i \quad (2)$$

$$\frac{dJ^i}{dt} = J^{pr}\ H\left(I_{N2}^{i},\ I_{0,J2}, n_{J2}, \lambda_{J2}\right) H\left(I_{N3}^{i},\ I_{0,J3}, n_{J3}, \lambda_{J3}\right) - J^i(k_c N_3^i + k_t N_{3,\ ext}^i) - J^i(k_c N_2^i + k_t N_{2,\ ext}^i) - \gamma J^i \quad (3)$$

$$I_{N3}^i = k_t\ N_3^i\ J_{ext}^i - \gamma_I\ I_{N3}^i \quad (4)$$

$$I_{N2}^i = k_t\ N_2^i\ J_{ext}^i - \gamma_I\ I_{N2}^i \quad (5)$$

Here, N_2, N_3, J represent the Notch2, Notch3, and Jagged1 protein levels, and I_{N3}, I_{N3} represent the NICD content of the cell. $N_2^{pr}, N_3^{pr}, J^{pr}$ are the basal production rates of Notch2, Notch3 and Jagged1, respectively. k_c, k_t denote the cis-inhibition and trans-activation strength parameters, respectively. γ represents the degradation rate of Notch and Jagged and γ_I is the degradation rate of NICD. The effects of transactivation on the production rate of Notch3 and Jagged1 from NICD2 and NICD3 were incorporated with shifted Hill functions in the following form:

$$H^S(ICD, \lambda, n) = \lambda + \frac{1-\lambda}{1+(\frac{I}{I_0})^n} \quad (6)$$

with I denoting the NICD content ($NICD_{N2}\ or\ NICD_{N3}$) and λ defining the changes in protein production in response to Notch2/Notch3 transactivation. The parameter I_0 defines the transition point of the Hill function from convex to concave and the parameter *n* determines the sensitivity of protein production to the NICD content. A schematic illustration of the interactions in the model is shown in Figure S3B.

The initial values for the protein content of Notch2, Notch3, Jagged, and NICD for each cell were randomly generated between 0 and 6000 molecules, similar to Loerakker et al.[13] and Ristori et al.[14]. The *trans* interactions occur with proteins located on the membranes of neighboring cells. Notch and Jagged were assumed to be distributed equally over the cell membrane, where half of the amount is available for binding with each of its neighbors. To replicate the experimental environment of a large number of closely packed cells in a cluster, periodic boundary conditions were applied to the first and last cells in the simulated array. Hence the first cell was treated as a neighbor to the last cell, creating a continuous loop, thereby eliminating artificial edge effects that would otherwise arise if the array had distinct boundaries (Figure S3C). For all other cells, the external Notch and Jagged were defined in the following form:

$$N_{ext}^i = \frac{N^{i+1} + N^{i-1}}{2} \quad (7)$$

$$J_{ext}^{i} = \frac{J^{i+1} + J^{i-1}}{2} + J^{coat} \quad (8)$$

Where N_{ext}^{i} and J_{ext}^{i} represent the external Notch[2/3] and Jagged1 for cell i that is available to for Jagged-Notch signaling, respectively, and J^{coat} is the constant external Jagged coating.

In line with the experimental conditions, we simulated three different protein manipulation setups: (1) Control, with both Notch2 and Notch3 production; (2) siN2, with Notch2 production knocked down; and (3) siN3, with Notch3 production knocked down. These three scenarios were also tested with external Jagged1 coating, resulting in three additional setups: Control_J, siN2_J, and siN3_J, giving a total of six experimental scenarios. Each simulation was repeated 25 times, and all simulations reached a steady-state solution after a simulated time of 15 hours. The stable protein content values in the periodic model were found to be insensitive to the to the time increment when chosen ≤0.01 of the explicit time integration scheme and the number of cells when chosen ≥10 cells, hence a time increment of 0.01 and 10 cells were adopted. The final protein production levels were averaged across cells and repeated simulations for each experimental scenario.

Most of the parameter values regulating the dynamics of Jagged1–Notch2/3 signaling in SMCs were adopted from Boareto et al.[96]. The basal production rates of Notch2 and Jagged1 were assumed to be half that of Notch3, which was set at 1000 h^{-1}, since based on RNAseq data, SMCs expressed 2-fold more copies of NOTCH3 than NOTCH2 at 24h (Figure S3 A). In addition, they seemed to express almost no other ligand than JAG1. The strengths of trans-activation (k_t) and cis-inhibition (k_c) were assumed 5×10^{-5} and 5×10^{-4}, respectively[13,96]. Hill function parameters were selectively optimized, with only the transition parameters $I0_{J3}$ *and* $I0_{N3}$ and sensitivity parameters n_{N2} *and* n_{N3} adopted from previous models[13,96]. The remaining parameters of the shifted Hill function were optimized to account for their potential influence on the results (see Table 1).

Table 1: Parameters of the shifted hill function characterizing the upregulation of Notch3 and Jagged 1 by NICD2 and NICD3 in the computational model.

Parameter	Description	Value/Range	Reference
λ_{N2}	Maximum fold change in **Notch** production rate from **Notch2**	To optimize [1,5]	
$I0_{N2}$	Transition parameter in **Notch** production rate from **Notch2**	To optimize [50,500]	
n_{N2}	Sensitivity parameter in **Notch** production rate from **Notch2**	2	13,95,96
λ_{N3}	Maximum fold change in **Notch** production rate from **Notch3**	To optimize [1.5,5]	50
$I0_{N3}$	Transition parameter in **Notch** production rate from **Notch3**	200	13,96
n_{N3}	Sensitivity parameter in **Notch** production rate from **Notch3**	2	13,95,96
λ_{J2}	Maximum fold change in **Jagged** production rate from **Notch2**	To optimize [1,5]	
$I0_{J2}$	Transition parameter in **Jagged** production rate from **Notch2**	To optimize [50,500]	
n_{J2}	Sensitivity parameter in **Jagged** production rate from **Notch2**	To optimize [1,10]	
λ_{J3}	Maximum fold change in **Jagged** production rate from **Notch3**	To optimize [1.5,5]	50
$I0_{J3}$	Transition parameter in **Jagged** production rate from **Notch3**	200	13,96
n_{J3}	Sensitivity parameter in **Jagged** production rate from **Notch3**	To optimize [1,10]	

We employed a Genetic Algorithm (GA) to optimize a set of eight parameters ($\lambda_{N2}, I0_{N2}, \lambda_{N3}, I0_{N3}, n_{N3}, \lambda_{J2}, I0_{J2}, n_{J2}, \lambda_{J3}, I0_{J3}, n_{J3}$) in the computational model of Notch signaling, aiming to minimize the Mean Squared Error (MSE) between simulated and experimental qPCR data at 24h from Figure 2 G for transmembrane proteins. The simulations were performed using MATLAB (The MathWorks Inc., v.R2025a). The objective function was defined to calculate the MSE between the normalized simulated outputs (averaged for cells at 24h) and the experimental data, using the Notch2-Notch3 signaling model. The GA was run with a maximum of 100 generations and the stopping criteria were set to three consecutive generations with no improvement, and a tolerance of 10^{-4}. The objective function calculated the Mean Squared Error (MSE) between simulated and experimental data for Notch2 (N2), Notch3 (N3) and Jagged1 (J1) relative expressions. As Notch2 is not influenced by Hill function parameters (Eq 2), the MSE was computed by summing the squared differences normalized values ($N_{3,j}^{sim}$ and J_j^{sim}) and ($N_{3,j}^{exp}$ $and\, J_j^{exp}$), where j denotes the index of the experimental scenario. Thus, the total MSE serves as the objective function (CF) that quantifies the difference between the two datasets.

$$N_{3,i}^{sim} = H\left(I_{N2}^{j},\ I_{0,N2}, n_{N2}, \lambda_{N2}\right) H\left(I_{N3}^{j},\ I_{0,N3}, n_{N3}, \lambda_{N3}\right) \tag{9}$$

$$J_j^{sim} = H\left(I_{N2}^{j},\ I_{0,J2}, n_{J2}, \lambda_{J2}\right) H\left(I_{N3}^{j},\ I_{0,J3}, n_{J3}, \lambda_{J3}\right) \tag{10}$$

$$MSE_{N3} = \sum_{i=1}^{6} (N_{3,i}^{sim} - N_{3,i}^{exp})^2 \tag{11}$$

$$MSE_J = \sum_{i=1}^{6} (J_i^{sim} - J_i^{exp})^2 \tag{12}$$

$$CF = MSE_{N3} + MSE_J \tag{13}$$

The optimization results including the best parameter values, number of iterations and the minimum cost value are given in Table 2

Table 2: Optimized parameters of the Notch signaling model using the Genetic Algorithm under constraints of Table 1.

Optimized Parameters								**Iterations**	**Cost**
$\boldsymbol{\lambda_{N2}}$	$\boldsymbol{I0_{N2}}$	$\boldsymbol{\lambda_{N3}}$	$\boldsymbol{\lambda_{J2}}$	$\boldsymbol{I0_{J2}}$	$\boldsymbol{n_{J2}}$	$\boldsymbol{\lambda_{J3}}$	$\boldsymbol{n_{J3}}$		
2.57	50.24	1.56	4.52	76.38	1.89	1.82	1.76	65	0.68

The optimization results showed a stronger influence of NICD2 on transmembrane protein production (Notch and Jagged), compared to that of NICD3 ($\lambda_{J2}, \lambda_{N2} > \lambda_{J3},\ \lambda_{N3}$). Additionally, $I0_{J2}$, $I0_{N2} < I0_{J3}, I0_{N3} = 200$, which shows that NICD2 induces Notch and Jagged at lower thresholds than those of NICD3. To verify these findings, we repeated the optimization procedure with constraints that enforced the opposite conditions:

(1) NICD3 was set to have a stronger influence on the production of Jagged1 and Notch3 than NICD2
($\lambda_{J3}, \lambda_{N3} > \lambda_{J2},\ \lambda_{N2}$)
(2) NICD3 was assumed to induce Notch3 and Jagged1 production at lower thresholds than NICD2

$$(I0_{J3}, I0_{N3} > I0_{J2},\ I0_{N2})$$

The results of the verification run are shown in Table 3, where both constraints led to significantly higher minimum costs in the optimization algorithm, indicating that these alternative scenarios deviated from the experimental mean protein levels (see Table 3 and Figure S3G).

Table 3: Optimized parameters of the Notch signaling model after enforcing opposite conditions of the original results from Table 2.

Optimized parameters								**Iterations**	**Cost**
$\boldsymbol{\lambda_{N2}}$	$\boldsymbol{I0_{N2}}$	$\boldsymbol{\lambda_{N3}}$	$\boldsymbol{\lambda_{J2}}$	$\boldsymbol{I0_{J2}}$	$\boldsymbol{n_{J2}}$	$\boldsymbol{\lambda_{J3}}$	$\boldsymbol{n_{J3}}$		
Condition 1: $\boldsymbol{\lambda_{J3}, \lambda_{N3} > \lambda_{J2},\ \lambda_{N2}}$									
1.85	74.18	1.88	2.47	50.3	5.02	2.68	1.19	16	2.25
Condition 2: $\boldsymbol{I0_{J3}, I0_{N3} > I0_{J2},\ I0_{N2}}$									
4.56	415	1.93	2.56	484.1	1.90	3.26	4.89	14	10.92

1D Model of Hybrid Arterial Wall

To simulate the Notch dynamics in smooth muscle cells (SMCs) within a *hybrid artery* — representing signaling under non-periodic boundary conditions replicating *in vivo* conditions—we adapted an existing computational framework, similar to previous studies[13,96], we assumed that the first cell in the linear arrangement is an endothelial cell that initiates the signaling cascade through constant emission of Jagged1 (Figure 4D). SMCs interact with each other as in the previous model, where trans interactions occur between proteins located on the membranes of adjacent cells. Notch and Jagged are both assumed to be evenly distributed across the cell membrane, with half of their total quantity available for binding with each neighboring cell.

Considering the significance of Notch in coronary artery dynamics , we selected the geometrical parameters for a coronary artery as the “hybrid artery” to be simulated, assuming an average wall thickness of 0.2 mm[97]. The simulated cell line consisted of 20 cells, assuming a cell size of 0.01mm consistent with the arterial thickness. The endothelial cell's constant Jagged1 emission rate was set to 4000 molecules/h, in agreement with previous studies[13,96].

FIGURES

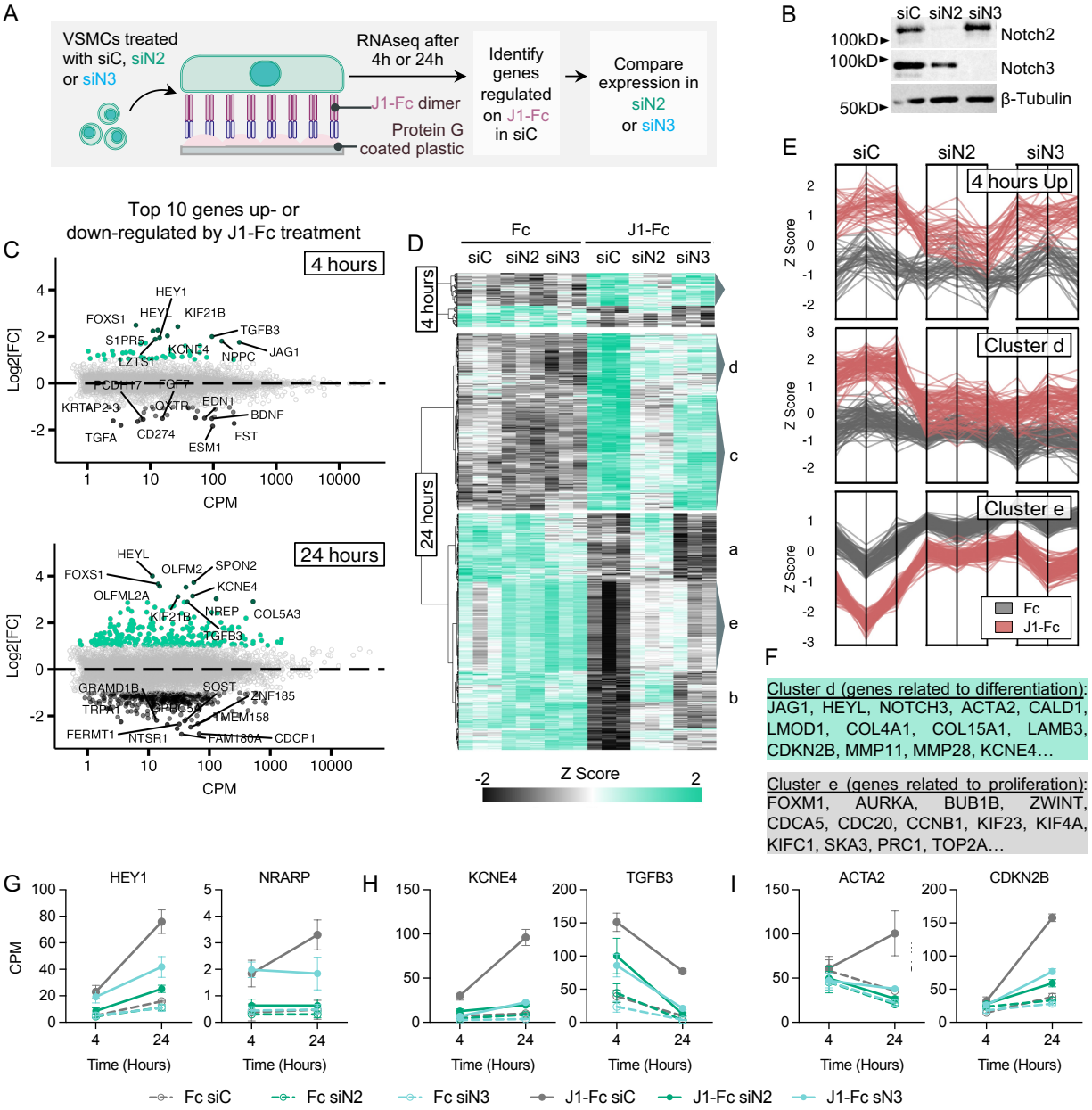
A
VSMCs treated with siC, siN2 or siN3
RNAseq after 4h or 24h
J1-Fc dimer
Protein G coated plastic
Identify genes regulated on J1-Fc in siC
Compare expression in siN2 or siN3
B
siC siN2 siN3
100kD
100kD
50kD
Notch2
Notch3
β-Tubulin
C
Top 10 genes up- or down-regulated by J1-Fc treatment
4 hours
24 hours
Log2[FC]
CPM
D
Fc
J1-Fc
siC siN2 siN3 siC siN2 siN3
4 hours
24 hours
Z Score
E
siC siN2 siN3
4 hours Up
Cluster d
Cluster e
Z Score
Fc
J1-Fc
F
Cluster d (genes related to differentiation): JAG1, HEYL, NOTCH3, ACTA2, CALD1, LMOD1, COL4A1, COL15A1, LAMB3, CDKN2B, MMP11, MMP28, KCNE4…
Cluster e (genes related to proliferation): FOXM1, AURKA, BUB1B, ZWINT, CDCA5, CDC20, CCNB1, KIF23, KIF4A, KIFC1, SKA3, PRC1, TOP2A…
G
HEY1
NRARP
H
KCNE4
TGFB3
I
ACTA2
CDKN2B
CPM
Time (Hours)
Fc siC
Fc siN2
Fc siN3
J1-Fc siC
J1-Fc siN2
J1-Fc sN3
J
sister chromatid segregation
mitotic nuclear division
nuclear division
nuclear chromosome segregation
chromosome segregation
granulocyte chemotaxis
chemokine-mediated signaling pathway
antimicrobial humoral immune response mediated by antimicrobial peptide
cardiac muscle tissue development
regulation of chondrocyte differentiation
muscle structure development
synaptic signaling
trans-synaptic signaling
anterograde trans-synaptic signaling
chemical synaptic transmission
blood circulation
circulatory system process
glomerulus development
G protein-coupled receptor signaling pathway
response to amphetamine
angiogenesis
blood vessel morphogenesis
glomerular epithelium development
chloride transport
p.adjust
0.025
0.050
0.075
GeneRatio
0.1
0.2
0.3
0.4
0.5

1272 Figure 1: Notch2 and Notch3 act as functional analogs during Jagged1-mediated SMC
1273 differentiation, but Notch2 facilitates the early transcriptional response.
1274
1275 (A) Schematic description of the experimental setup and the analysis strategy for the RNAseq
1276 experiment.
1277 (B) Notch2 and Notch3 protein levels in SMCs 48h post-transfection with the corresponding
1278 siRNAs.
1279 (C) Genes significantly regulated in SMCs on immobilized J1-Fc at 4h and 24h (FC>2,
1280 FDR>0.05) based on RNAseq. The top 10 up- or downregulated genes are annotated (n=3
1281 independent experiments).
1282 (D) Heatmaps clustered by Ward´s method showing the z-scores of genes regulated in SMCs
1283 on immobilized J1-Fc at 4h and 24h time points across cells treated with control, Notch2 or
1284 Notch3 siRNAs (n=3 independent experiments). Gene clusters were considered as follows:
1285 Cluster c; upregulated more by Notch2 and less by Notch3, cluster d; upregulated by both
1286 Notch2 and Notch3, and Cluster e; downregulated both by Notch2 and Notch3.
1287 (E) Behavior of the gene clusters upon different treatments: genes upregulated on immobilized
1288 J1-Fc at 4h, 24h cluster d, and 24h cluster e, respectively.
1289 (F) Lists of representative genes related to SMC differentiation and extracellular matrix
1290 production upregulated on J1-Fc (Cluster d) and genes related to proliferation downregulated on
1291 J1-Fc (Cluster e).
1292 (G-I) Expression of genes representative of Notch signaling activity, contractile differentiation,
1293 and cell cycle arrest (mean±SD).
1294 (J) Gene ontology analysis of the clusters from 24h as listed by the “clusterprofiler” package.

1295

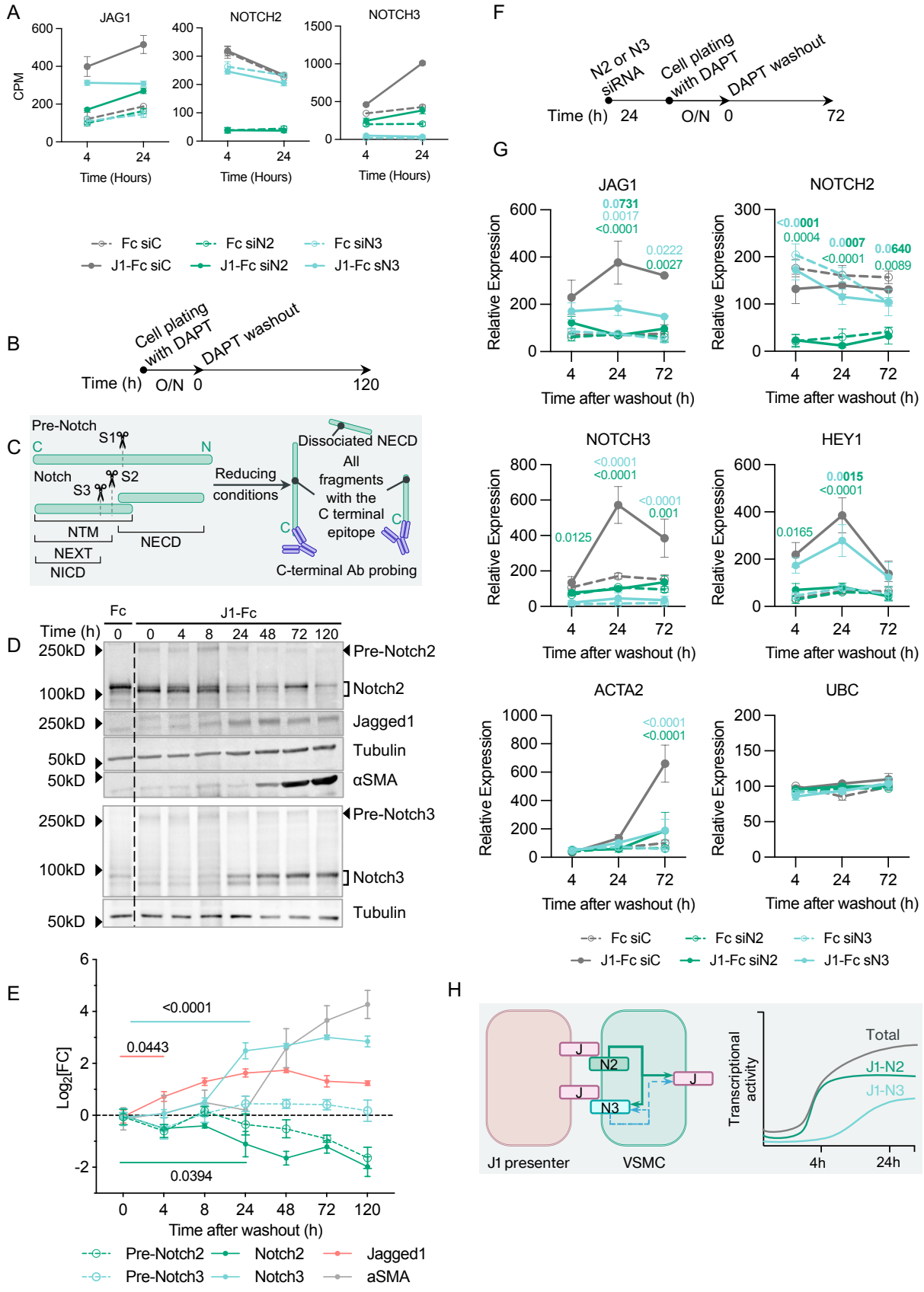
A
JAG1
NOTCH2
NOTCH3
CPM
Time (Hours)
Fc siC
Fc siN2
Fc siN3
J1-Fc siC
J1-Fc siN2
J1-Fc sN3
B
Cell plating with DAPT
DAPT washout
Time (h)
O/N
0
120
C
Pre-Notch
S1
C
N
Notch
S2
S3
NTM
NECD
NEXT
NICD
Reducing conditions
Dissociated NECD
All fragments with the C terminal epitope
C-terminal Ab probing
D
Fc
J1-Fc
Time (h)
0
4
8
24
48
72
120
250kD
100kD
50kD
Pre-Notch2
Notch2
Jagged1
Tubulin
αSMA
Pre-Notch3
Notch3
E
Log2[FC]
<0.0001
0.0443
0.0394
Time after washout (h)
Pre-Notch2
Notch2
Jagged1
Pre-Notch3
Notch3
aSMA
F
N2 or N3 siRNA
Cell plating with DAPT
DAPT washout
Time (h)
24
O/N
0
72
G
JAG1
NOTCH2
NOTCH3
HEY1
ACTA2
UBC
Relative Expression
Time after washout (h)
0.0731
0.0017
<0.0001
0.0222
0.0027
<0.0001
0.0004
0.0007
<0.0001
0.0640
0.0089
<0.0001
<0.0001
0.0125
<0.0001
0.001
0.0015
<0.0001
0.0165
<0.0001
<0.0001
Fc siC
Fc siN2
Fc siN3
J1-Fc siC
J1-Fc siN2
J1-Fc sN3
H
J
N2
N3
J1 presenter
VSMC
Transcriptional activity
Total
J1-N2
J1-N3
4h
24h

Figure 2: The Jagged1-Notch2 axis upregulates Notch3 for the progression of the differentiation program.

(A) Expression of NOTCH2 and NOTCH3 mRNA across the groups during the RNAseq experiment (mean±SD, n=3 independent experiments).
(B) *The DAPT washout experiment setup was used for the analysis of the Notch protein levels during the J1-Fc mediated differentiation.*
(C) Schematic description of the probing method used for detecting the Notch receptor products. Using antibodies against epitopes on the C-terminal end of the Notch receptor peptides allows for the detection of fragments, namely, Pre-Notch (non-membranous Notch protein that has not gone through S1-cleavage), NTM (S1-cleaved Notch transmembrane-intracellular domain), and NEXT (S2-cleaved Notch extracellular-truncated intracellular domain). In reducing lysis conditions, the NTM and the NECD (Notch extracellular domain) that are held together via physical bonds dissociate. Thus, here the NTM and its products were used to assess the levels of the mature membranous Notch receptor.
(D, E) The immunoblot analysis (D) and the quantified signal from the indicated proteins relative to the protein loading (E) in SMCs plated on immobilized J1-Fc over five days. The dotted lines represent log2 fold change (mean±*SEM, n=3 independent experiments, one-way repeated measures ANOVA, and Dunnet´s test for multiple comparisons. Pairwise comparisons with p values smaller than 0.1 are indicated on the plot).*
(F, G) The setup used for the DAPT washout experiment to assess the impact of Notch2 or Notch3 knockdown on Notch signaling in SMCs plated on immobilized J1-Fc and the qPCR analysis (E) for the indicated mRNA levels. The dotted lines represent relative expression (mean±SEM, n=3 independent experiments (n=2 for 72h). Two-way ANOVA and Tukey´s test for multiple comparisons were performed individually for different time points. Pairwise comparisons between J1-Fc-treated samples with p values smaller than 0.1 are indicated on the plots and color-coded for the groups compared).
(H) Schematic description of the working model regarding the temporal relationship between Jagged1, Notch2, and Notch3 and the Notch signaling output over time-based on figures 1,2, and S3.

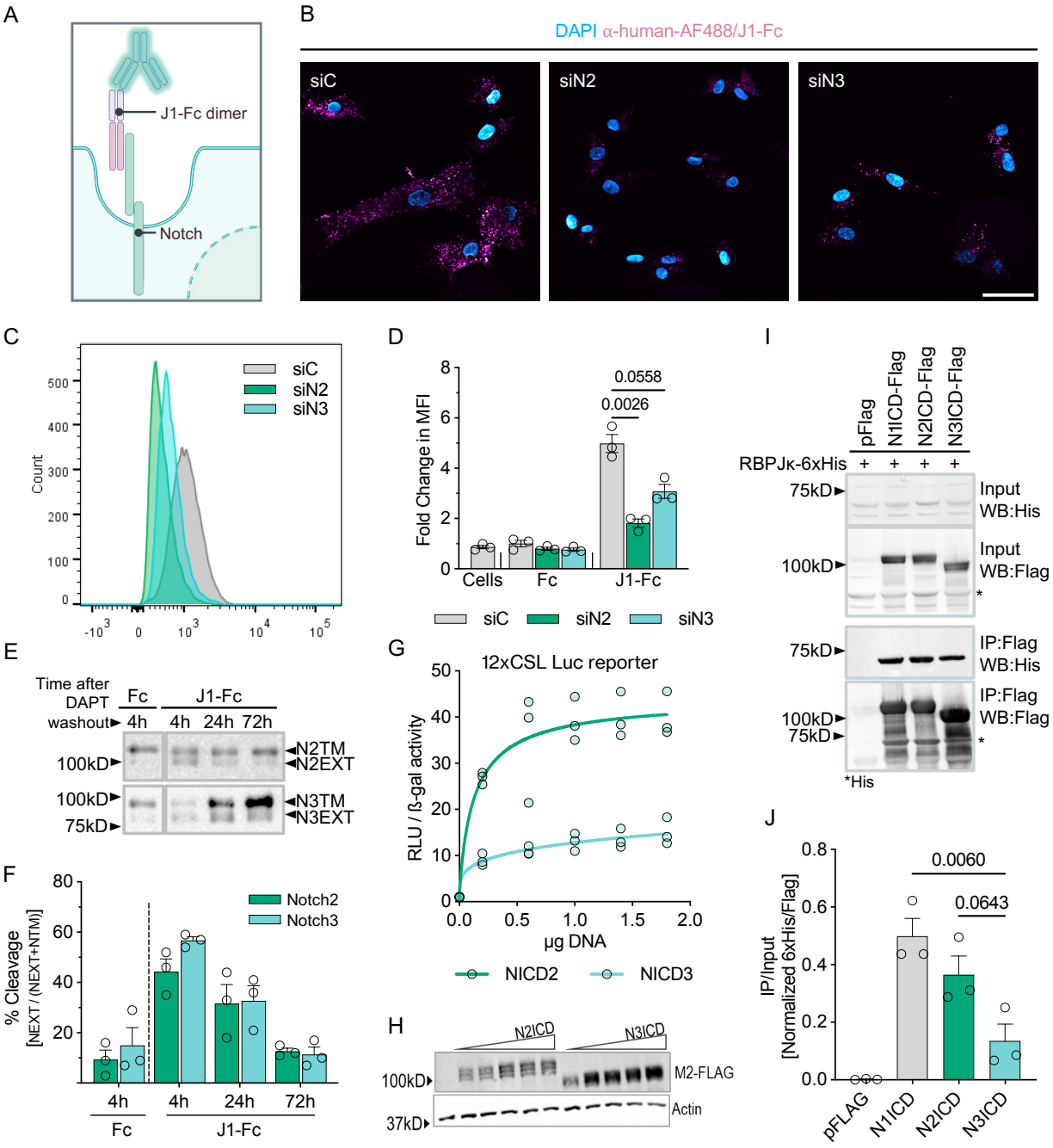
A
J1-Fc dimer
Notch
B
DAPI α-human-AF488/J1-Fc
siC
siN2
siN3
C
siC
siN2
siN3
Count
D
Fold Change in MFI
0.0558
0.0026
Cells
Fc
J1-Fc
siC
siN2
siN3
E
Time after DAPT washout
Fc
J1-Fc
4h
4h
24h
72h
100kD
N2TM
N2EXT
100kD
75kD
N3TM
N3EXT
F
% Cleavage [NEXT / (NEXT+NTM)]
Notch2
Notch3
4h
4h
24h
72h
Fc
J1-Fc
G
12xCSL Luc reporter
RLU / ß-gal activity
µg DNA
NICD2
NICD3
H
N2ICD
N3ICD
100kD
M2-FLAG
37kD
Actin
I
pFlag
N1ICD-Flag
N2ICD-Flag
N3ICD-Flag
RBPJκ-6xHis
75kD
Input WB:His
100kD
Input WB:Flag
75kD
IP:Flag WB:His
100kD
75kD
IP:Flag WB:Flag
*His
J
IP/Input [Normalized 6xHis/Flag]
0.0060
0.0643
pFLAG
N1ICD
N2ICD
N3ICD

1327

Figure 3: Elevated levels of Notch3 are required for transcriptionally meaningful canonical Notch3 signaling due to the weak Notch3-CSL interaction.

(A) Schematic representation of the live staining of Notch receptors in the SMCs with labeled soluble J1-Fc.

(B) Confocal slices of formalin-fixed SMCs (control, Notch2KD, and Notch3KD) following live staining with J1-Fc (Scale bar=50μm).

(C, D) Representative histograms and the bar plots (D) showing the fold change in mean intensity of live cells stained with J1-Fc measured using FACS (mean+SEM, n=3 independent experiments, one-way ANOVA followed by Šídák's test for multiple comparisons. Pairwise comparisons between J1-Fc-stained samples with p values lower than 0.1 are shown on the plot.).

(E, F) Immunoblots produced by C-terminal probing of Notch2 and Notch3 following DAPT washout in SMCs plated on immobilized J1-Fc, and the quantitative analysis of the bands. (F)The receptor cleavage was measured by the ratio of the NEXT (lower band) to the total S1-processed fragment (NEXT+TMIC (higher band)) (mean+SEM, n=3 independent experiments, one-way ANOVA followed by Šídák's test for multiple comparisons. Pairwise comparisons with p values lower than 0.1 are shown on the plot.).

(G, H) CSL-dependent Notch transcriptional activity in HEK 293T cells transfected with increasing amounts of Flag-tagged Notch2 or Notch3 ICD and 12xCSL-luciferase. The luciferase activity is presented as luminescence intensity relative to β-galactosidase activity. The immunoblots show the expression of the NICD-Flag constructs relative to β-tubulin (H). (mean+SEM, n=3 independent experiments. Data are presented as regression curves and circles as replicates.).

(I, J) Flag-tagged NICD paralogs were immunoprecipitated from HEK 293T cells co-expressing 6xHis-tagged RBPJκ. The Flag and the 6xHis IP signals were normalized to the input. The normalized 6xHis/Flag signal is presented in the bar plot (J) (mean+SEM, n=3 independent experiments, one-way ANOVA followed by Tukey's test for multiple comparisons. Pairwise comparisons between NICD paralogs with p values lower than 0.1 are shown on the plot.).

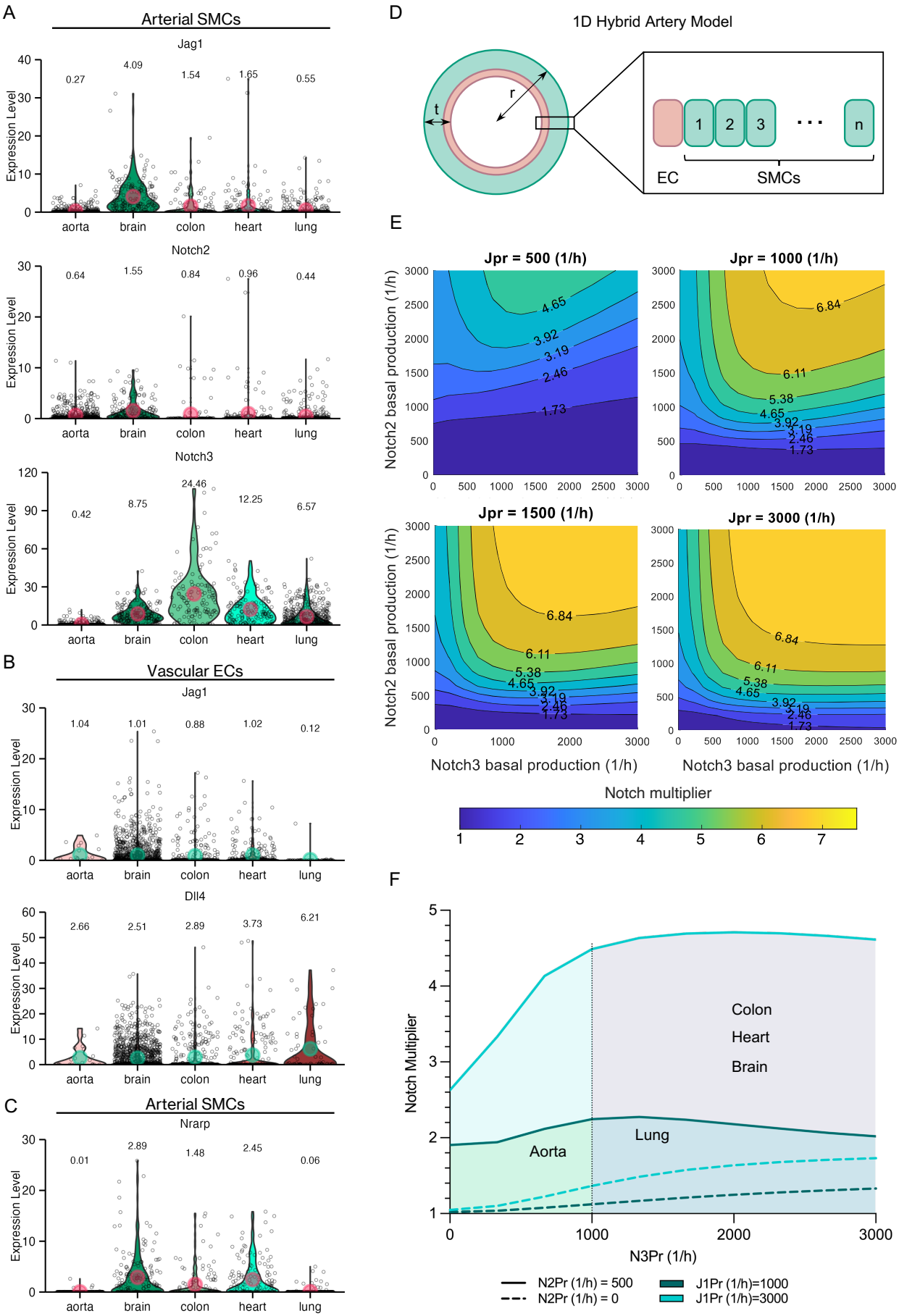
A
Arterial SMCs
Jag1
Expression Level
0.27
4.09
1.54
1.65
0.55
aorta
brain
colon
heart
lung
Notch2
0.64
1.55
0.84
0.96
0.44
Notch3
0.42
8.75
24.46
12.25
6.57
B
Vascular ECs
Jag1
1.04
1.01
0.88
1.02
0.12
Dll4
2.66
2.51
2.89
3.73
6.21
C
Arterial SMCs
Nrarp
0.01
2.89
1.48
2.45
0.06
D
1D Hybrid Artery Model
t
r
1
2
3
n
EC
SMCs
E
Jpr = 500 (1/h)
Jpr = 1000 (1/h)
Jpr = 1500 (1/h)
Jpr = 3000 (1/h)
Notch2 basal production (1/h)
Notch3 basal production (1/h)
4.65
3.92
3.19
2.46
1.73
6.84
6.11
5.38
Notch multiplier
F
Notch Multiplier
N3Pr (1/h)
Colon
Heart
Brain
Lung
Aorta
N2Pr (1/h) = 500
N2Pr (1/h) = 0
J1Pr (1/h)=1000
J1Pr (1/h)=3000

1358 *Figure 4: Levels of Notch3 predict artery-typical vulnerability to altered Jagged1-Notch2/Notch3*
1359 *signaling in the SMCs.*
1360 *(A-C) Normalized expression of Notch signaling components and Notch target gene Nrarp in*
1361 *arterial SMCs (A and C) and vascular endothelial cells (B) of different mouse organs extracted*
1362 *from scRNAseq data (Muhl et al.[36]; aorta, heart, colon, and lung) and (Vanlandewijck et al.[60];*
1363 *brain). The circles and the text above the violin plots denote the mean expression.*
1364 *(D) Schematic one-dimensional array of 1D artery model with an endothelial cell and a row of*
1365 *SMCs. The cascade of signaling is initiated by constant Jagged1 emission from the endothelial*
1366 *cell (EC) and SMCs are interacting with their neighboring cells.*
1367 *(E) Heatmaps showing the simulated impact of the initial Jagged1, Notch2, and Notch3 levels*
1368 *on the Notch signaling readout (Notch multiplier) in the 1D hybrid arterial wall.*
1369 *(F)2D projection of the predicted ranges of Notch multiplier in arterial SMCs of different organs*
1370 *with respect to their stoichiometrically scaled levels of Jagged1, Notch2, and Notch3 based on*
1371 *A, and in a Notch2 knockout scenario.*

1372

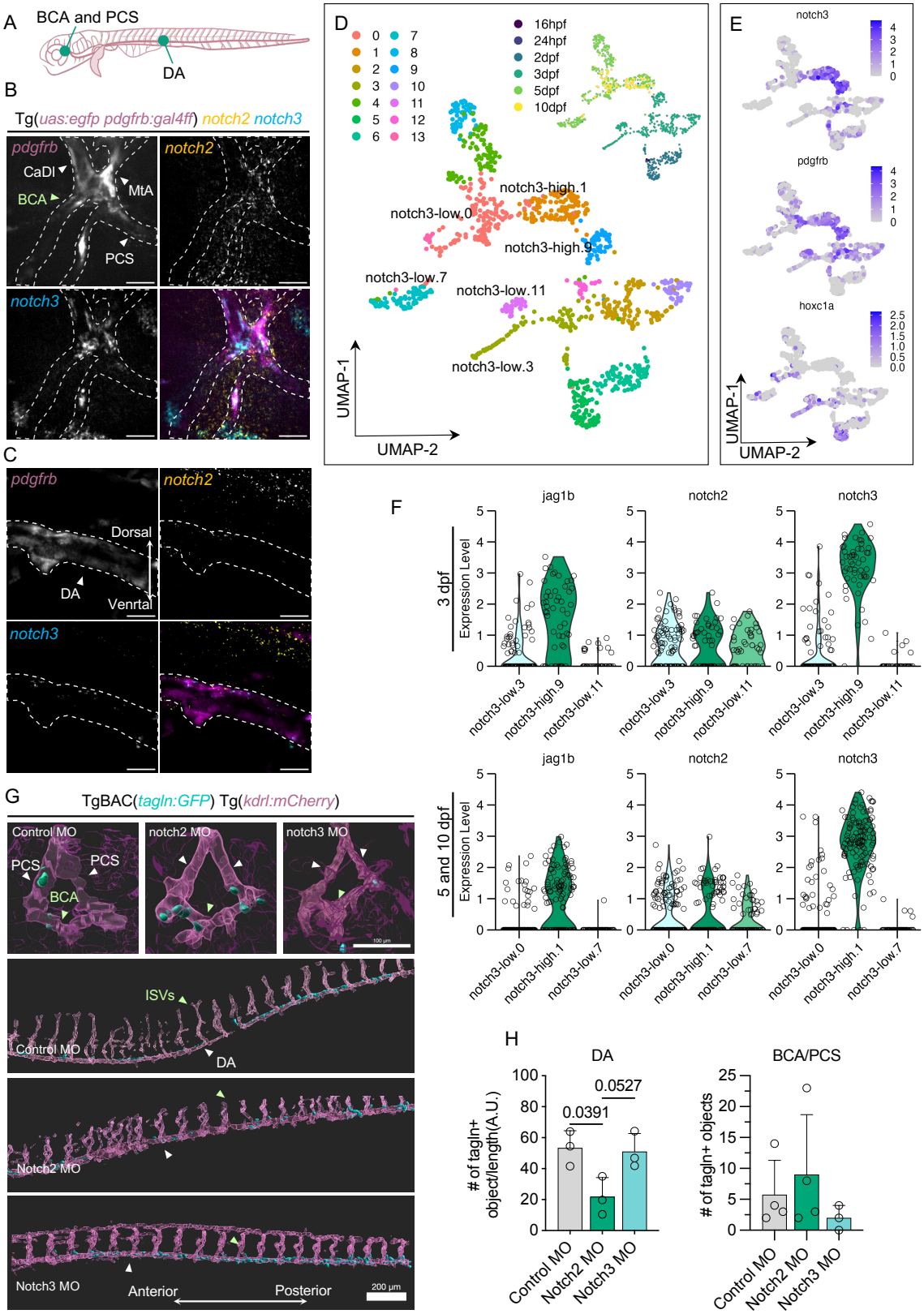
A
BCA and PCS
DA
B
Tg(uas:egfp pdgfrb:gal4ff) notch2 notch3
pdgfrb
CaDI
MtA
BCA
PCS
notch2
notch3
C
pdgfrb
notch2
Dorsal
DA
Venrtal
notch3
D
0 1 2 3 4 5 6 7 8 9 10 11 12 13
16hpf
24hpf
2dpf
3dpf
5dpf
10dpf
notch3-high.1
notch3-low.0
notch3-high.9
notch3-low.7
notch3-low.11
notch3-low.3
UMAP-1
UMAP-2
E
notch3
pdgfrb
hoxc1a
UMAP-1
UMAP-2
F
jag1b
notch2
notch3
3 dpf
Expression Level
notch3-low.3
notch3-high.9
notch3-low.11
5 and 10 dpf
notch3-low.0
notch3-high.1
notch3-low.7
G
TgBAC(tagln:GFP) Tg(kdrl:mCherry)
Control MO
notch2 MO
notch3 MO
PCS
BCA
ISVs
DA
Notch3 MO
Anterior
Posterior
200 µm
H
DA
BCA/PCS
# of tagln+ object/length(A.U.)
# of tagln+ objects
0.0391
0.0527
Control MO
Notch2 MO
Notch3 MO

1373

Figure 5: Artery-typical elevated Notch3 expression in the developing SMCs can compensate for Notch2 depletion in the zebrafish larvae (Created with Biorender).

(A) Schematic description of the vascular tree of the zebrafish larvae, and the position of the DA, the PCS, and the BCA (Created using Biorender).

(B, C) In situ RNA HCR was performed with probes against notch2 and notch3 in 3dpf zebrafish larvae bearing a pdgfrb reporter. Maximum intensity projections of five slice-thick confocal sections of the arteries from the cerebral base (B) and the dorsal aorta (C) given with dashed lines loosely marking the arterial regions based on the pdgfrb signal are shown (Scale bars=20 µm) (DA: dorsal aorta, BCA: basal communicating artery, PCS: posterior communicating segment, CaDI: caudal division of the internal carotid artery, MtA: metencephalic artery)

(D) UMAP projection of the SMCs color-coded based on the Seurat clusters and the developmental stage from the Zebrahub mesoderm scRNAseq dataset[69]. Cluster annotations were based on known markers of vascular and non-vascular SMCs as well as notch3 expression (Please see Figure 5S). The vascular SMCs were annotated based on the time point and notch3 expression status (high or low).

(E, F) Normalized expression of notch3, the general mural marker pdgfrb, the anteroposterior position-related homeobox gene hoxc1a; and (F) the normalized expression of the Notch signaling components in the indicated vascular SMC clusters at developmental stages relevant for mural cell emergence.

(G, H) The embryos bearing a contractility reporter (tagln:GFP) or the endothelial reporter (kdrl:mCherry) were injected with 10ng control, notch2 or notch3 morpholinos. The orthogonal view of the surface-rendered light sheet images of the indicated arteries from the 102 hpf (G, the BCA/PCS, scale bar=100µm and H, the DA and the ISV, scale bar=200µm). The number of tagln+ objects associated with the endothelium are shown in the bar plots (H) (n=3 or 4 embryos per morphant group, one-way ANOVA followed by Tukey´s test for multiple comparisons. Pairwise comparisons with p values smaller than 0.1 are shown on the plots.).

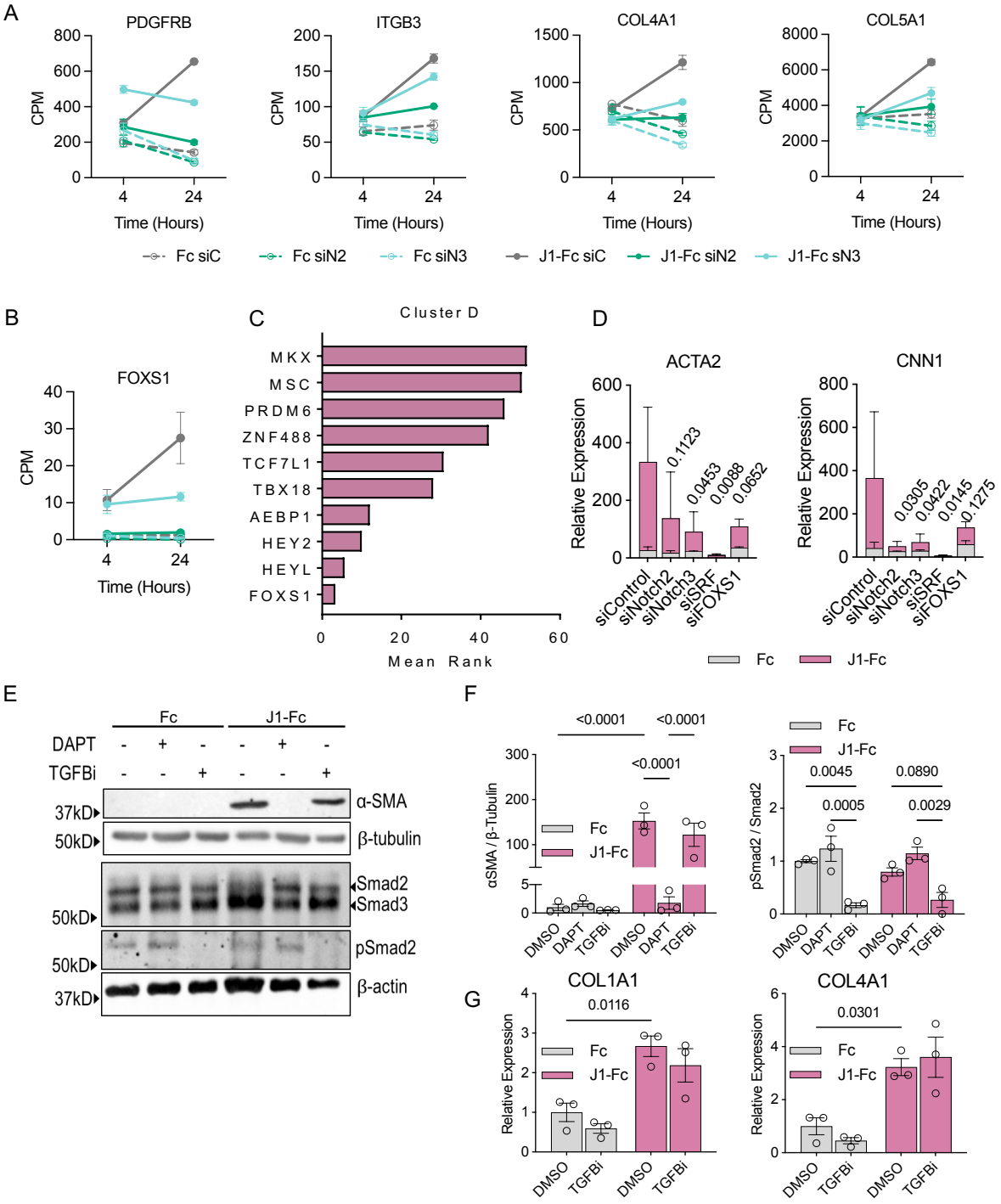
A
PDGFRB
ITGB3
COL4A1
COL5A1
CPM
Time (Hours)
Fc siC
Fc siN2
Fc siN3
J1-Fc siC
J1-Fc siN2
J1-Fc sN3
B
FOXS1
C
Cluster D
MKX
MSC
PRDM6
ZNF488
TCF7L1
TBX18
AEBP1
HEY2
HEYL
FOXS1
Mean Rank
D
ACTA2
CNN1
Relative Expression
siControl
siNotch2
siNotch3
siSRF
siFOXS1
Fc
J1-Fc
E
DAPT
TGFBi
37kD
50kD
α-SMA
β-tubulin
Smad2
Smad3
pSmad2
β-actin
F
αSMA / β-Tubulin
pSmad2 / Smad2
DMSO
DAPT
TGFBi
G
COL1A1
COL4A1

Supplementary Figure S1: Notch2 and Notch3 both act upstream of genes associated with Jagged1-driven periarterial coverage and maturation (Related to Figure 1).
(A) Selected genes from cluster c, regulated by Jagged1-Notch2/Notch3 signaling associated with SMC growth and extracellular matrix production based on RNAseq.
(B) Expression of FOXS1, based on RNAseq. FOXS1 was one of the top 10 upregulated genes by J1-Fc stimuli at both time points (please see also Figure 1 C and D) (mean+SD, n=3 independent experiments).
(C) Genes from RNAseq cluster d were analyzed for transcription factor co-expression using the ChEA3 web tool. The top 10 possible upstream transcription factors as listed by ChEA3 are listed with their mean rank (the lower the better) in the bar chart.
(D) SMCs were treated with the indicated siRNAs for 48h and grown on immobilized J1-Fc for another 48h. The indicated mRNAs were analyzed using qPCR, normalized to UBC, and presented as relative expression (mean+SEM, n=2 independent experiments, one-way ANOVA followed by Dunnett´s test for multiple comparisons to the J1-Fc siControl. The comparisons of J1-Fc-treated samples with p values smaller than 0.1 are shown on the corresponding bars).
(E-G) SMCs were grown on immobilized J1-Fc (72h for WB and 24h for qPCR) with 10μM DAPT, TGFβi, or DMSO and analyzed for the indicated molecules. The αSMA and phopho-Smad2 signals were normalized to β-tubulin, and total Smad2, respectively, and presented as fold change (F). For qPCR, the relative expression was normalized to UBC and presented as fold change (G) (n=3 independent experiments, one-way ANOVA followed by Šídák's test for multiple comparisons. Pairwise comparisons with p values smaller than 0.1 are shown on the plots.).

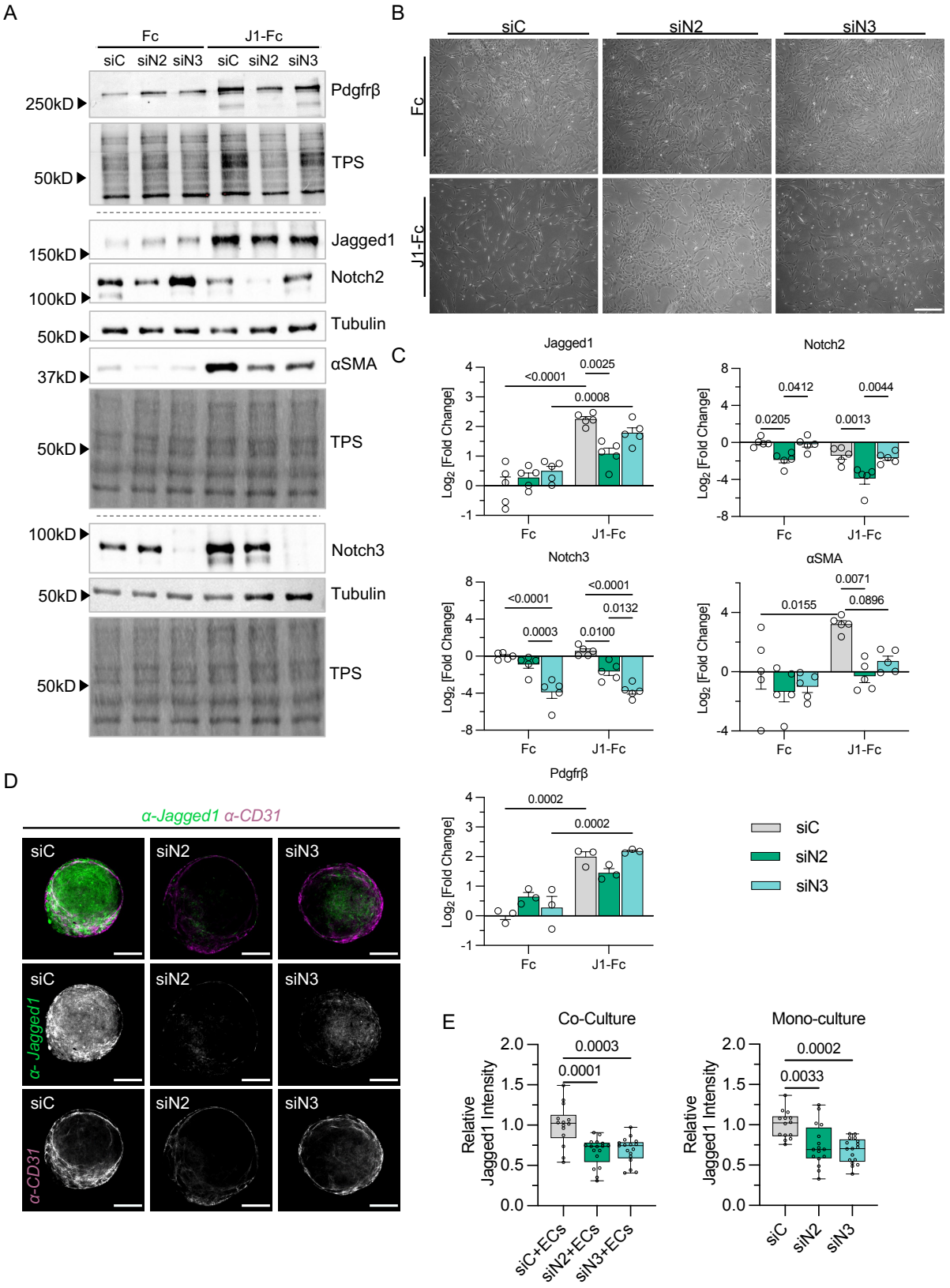
A
Fc
J1-Fc
siC siN2 siN3 siC siN2 siN3
250kD
Pdgfrβ
50kD
TPS
150kD
Jagged1
100kD
Notch2
50kD
Tubulin
37kD
αSMA
50kD
TPS
100kD
Notch3
50kD
Tubulin
50kD
TPS
B
siC
siN2
siN3
Fc
J1-Fc
C
Jagged1
Notch2
Notch3
αSMA
Pdgfrβ
Log2 [Fold Change]
Fc
J1-Fc
siC
siN2
siN3
D
α-Jagged1 α-CD31
siC
siN2
siN3
α- Jagged1
α-CD31
E
Co-Culture
Mono-culture
Relative Jagged1 Intensity
siC+ECs
siN2+ECs
siN3+ECs
siC
siN2
siN3

1426 *Supplementary Figure S2: Late Notch3 activity is important for the contractile differentiation*
1427 *(Related to Figures 1 and 2)*
1428 *(A-C) SMCs were treated with the indicated siRNAs for 48h and grown on immobilized J1-Fc for*
1429 *72h (B) before immunoblotting for the indicated proteins(A). The signal was normalized to*
1430 *protein loading and presented as log2 fold change(C) (mean+SEM, n=5 (n=3 for Pdgfrβ)*
1431 *independent experiments, two-way ANOVA followed by Tukey´s test for multiple comparisons.*
1432 *Pairwise comparisons with p values lower than 0.1 are indicated on the plots).*
1433 *(D, E) Notch2KD or Notch3KD SMCs were grown as spheroids in low-adhesion U-bottom plates*
1434 *for 72h (monoculture) or 48h before another 24h with human umbilical vein endothelial cells (co-*
1435 *culture). The spheroids were fixed and stained for Jagged1 or CD31. The representative*
1436 *confocal slices (D) and their mean Jagged1 intensity are shown (E) (Scale bars=150µm, error*
1437 *bars represent the min-max range, n=3 independent experiments with at least 4 spheroids per*
1438 *condition, one-way ANOVA followed by Tukey´s test for multiple comparisons. Pairwise*
1439 *comparisons with p values lower than 0.1 are indicated on the plots.).*

1440

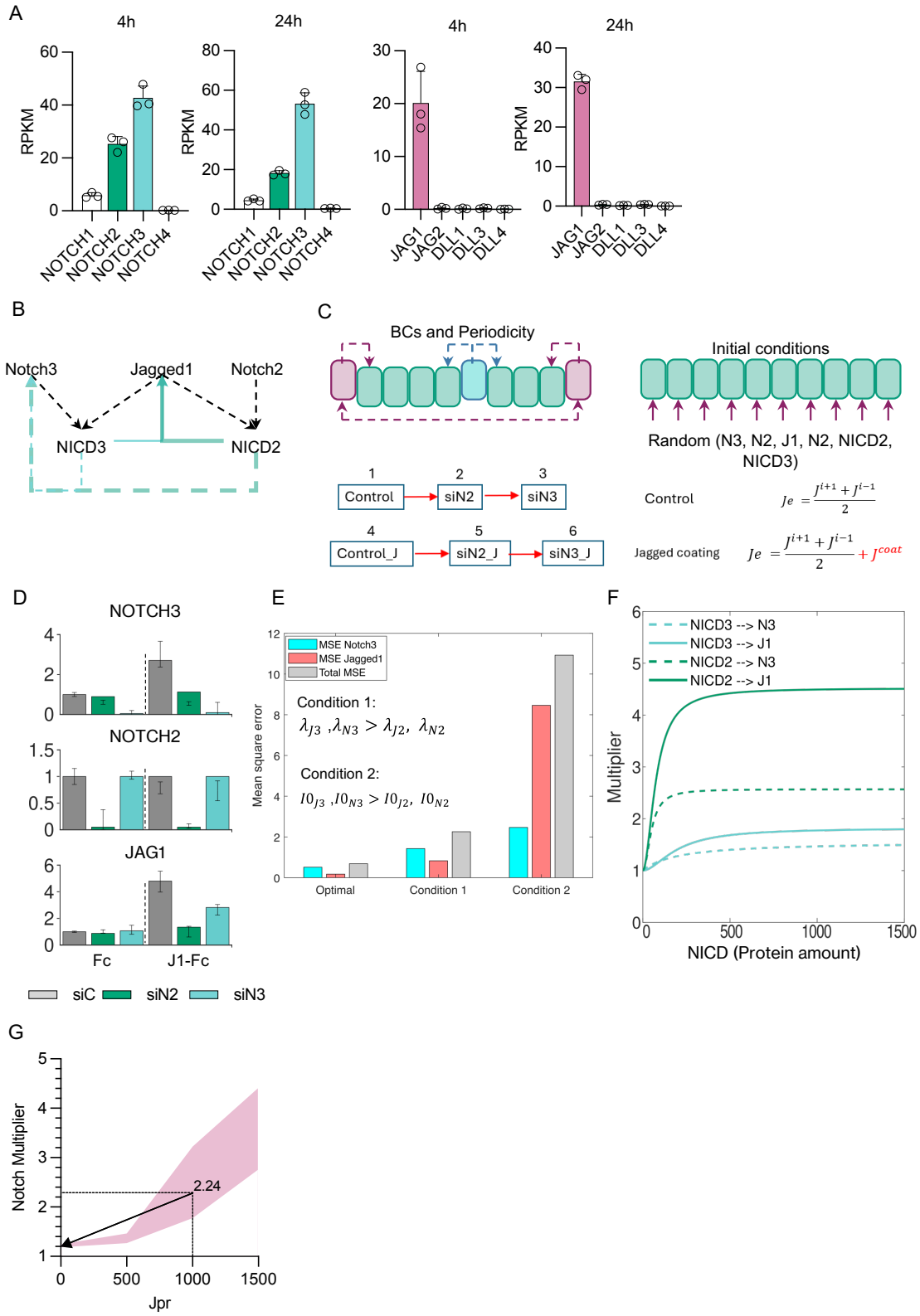
A
4h
24h
4h
24h
RPKM
NOTCH1
NOTCH2
NOTCH3
NOTCH4
JAG1
JAG2
DLL1
DLL3
DLL4
B
Notch3
Jagged1
Notch2
NICD3
NICD2
C
BCs and Periodicity
Initial conditions
Random (N3, N2, J1, N2, NICD2, NICD3)
Control
siN2
siN3
Control_J
siN2_J
siN3_J
Jagged coating
D
NOTCH3
NOTCH2
JAG1
Fc
J1-Fc
siC
siN2
siN3
E
MSE Notch3
MSE Jagged1
Total MSE
Mean square error
Condition 1:
Condition 2:
Optimal
Condition 1
Condition 2
F
NICD3 --> N3
NICD3 --> J1
NICD2 --> N3
NICD2 --> J1
Multiplier
NICD (Protein amount)
G
Notch Multiplier
2.24
Jpr

1441

Supplementary Figure S3 (Related to Figure 3 and Figure 4):
(A) Basal expression of different Notch receptors and ligands in SMCs at 4h and 24h siC- and Fc-treated SMCs based on RNAseq.
(B) Diagram depicting the causative relationship between Notch2, Notch3, and Jagged1 included in the theoretical framework used for building the computational model. Line weight denotes the strength of the interaction as informed by the experimental data from Figure 2.
(C) Schematic one-dimensional array of vascular SMCs with periodic boundary conditions and initial random values of transmembrane and intracellular proteins (top). Experimental scenarios of protein manipulation with and without jagged coating with external jagged derivation for the cell (bottom).
(D) Model validation was performed by enforcing assumptions (conditions 1 and 2) opposite to those the experimental data suggests (optimal). The simulated means against the experimental data (error bars) and the mean squared error for each condition are presented as bar plots.
(E) Simulated results from the model showing the levels of the Notch signaling components in response to Jagged1 stimuli following parameter optimization. Bars and error bars represent simulated fold changes and the standard error in fold changes from the experimental data (24h) from Figure 2 G.
(F) Hill curves resulting from the simulation with optimized parameters, showing the causative effect of Notch2 or Notch3 ICD on the production of Jagged1 and Notch3 as Notch signaling targets.
(G) The predicted Notch signaling multiplier range in the aortic SMCs, was calculated using the ranges N2pr(428:642)(1/h) and N3Pr(857:1071)(1/h). Using N2Pr=500, N3Pr=1000, and Jpr=1000 produces a multiplier of 2.24. Jpr=0 reduces the multiplier to approximately 1.

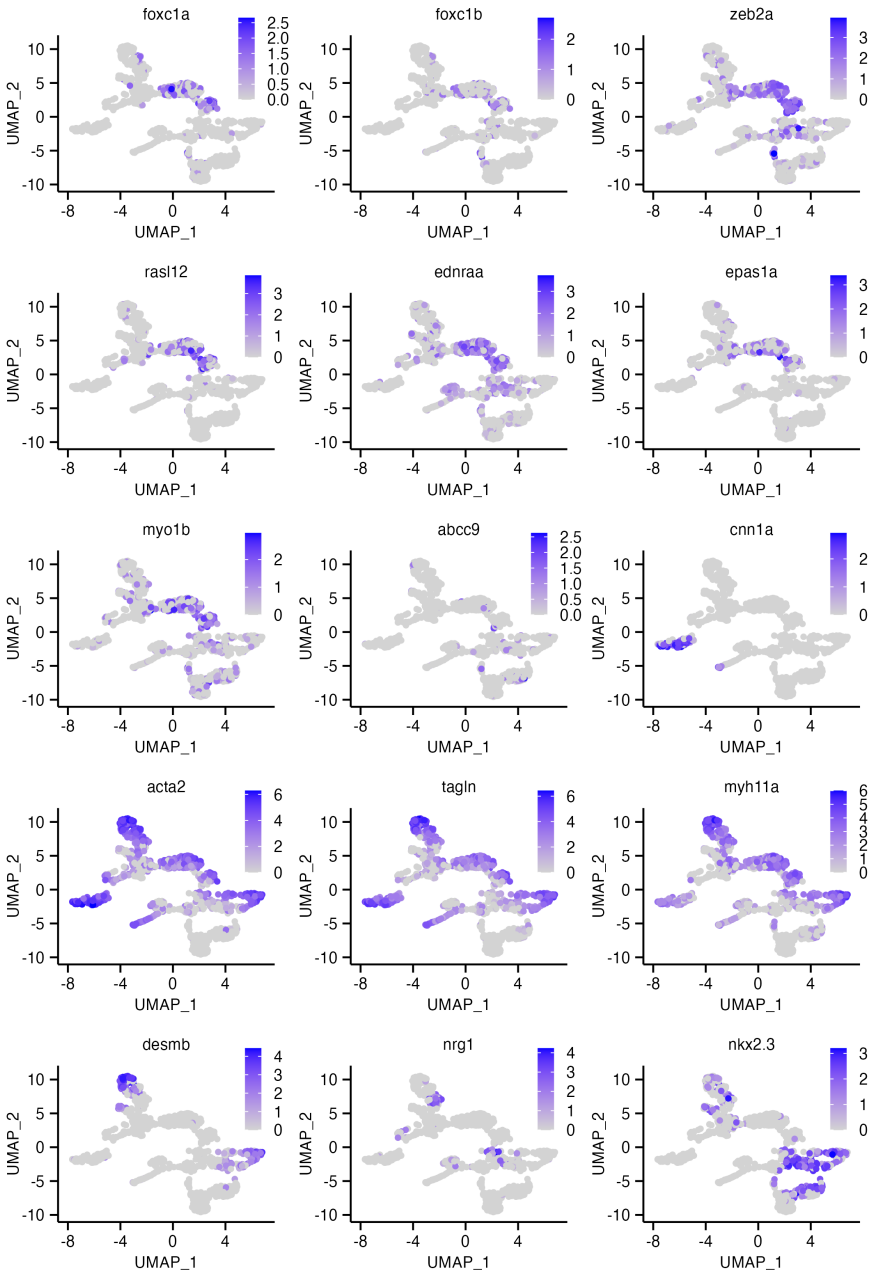

Supplementary Figure S4 (Related to Figure 5):

Genes enriched in the notch3-high SMC clusters (foxc1a, foxc1b, zeb2a, rasl12, ednraa, epas1a, myo1b), and markers used for annotating pericytes (abcc9), smooth muscle (cnn1a, acta2, tagln, myh11a), and visceral muscle (desmb, nrg1, and nkx2.3).

1472 *Resources table*

REAGENT or RESOURCE	SOURCE	IDENTIFIER
BIOLOGICAL MODELS		
Human aortic smooth muscle cells	Lonza	Cat #CC2571 (Lot #0000369150 Age 43, Male)
Human aortic smooth muscle cells	Lonza	Cat #CC2571 (Lot #0000335663 Age 22, Male)
Human aortic smooth muscle cells	ATCC	Cat #PCS-100-012™ (Lot 80126171, Age 23, Female)
Human umbilical vein endothelial cells	Promocell	Cat #C-12200 (Lot info NA)
HEK 293T cells	NA	NA
Tg(tagln:GFP)	Turku Bioscience Zebrafish Core Facility	Ando et al.[98]
Tg(kdrl:mCherry)		Ando et al.[98]
Tg(UAS:EGFP, pdgfrb:GAL4FF)		NA
REAGENTS		
Dulbecco´s Modified Eagle´s Medium	Merck	Cat #D6429
Opti-MEM	Gibco	Cat #31985062
ReagentPack™ for subculturing	Lonza	Cat #CC50-34
Fetal Bovine Serum	Gibco	Cat #17914671
Goat Serum	Biowest	Cat #S2000
Bovine Serum Albumin	Merck	Cat #A9418
L-glutamine	Merck	Cat #G7513
Penicillin/Streptomycin	Merck	Cat #P0781
PBS	Biowest	Cat #L0616
Revert™ 700 Total Protein Stain	LI-COR	Cat # 926-11016
NucleoSpin RNA	Macharey-Nagel	Cat #740955
SensiFAST™ cDNA Synthesis Kit	Bioline	Cat #Bio-65054
RNAiMAX Lipofectamine®	Thermo Fisher Scientific	Cat #13778150
JetOTIMUS®	Sartorius	Cat #101000006
SB-431542	MedChem Express	Cat #HY-10431
DAPT ((2S)- N- [(3,5-Difluoro phenyl)acetyl]- L-alanyl- 2-phenyl]glycine 1,1-dimethyl ethyl ester)	Bio-Techne	Cat # 2634-10

RNAScope™ Protease Plus	Bio-Techne	Cat #322331
HCR™ Gold RNA	Molecular Instruments	NA
5x HOT FIREPol EvaGreen qPCR Mix Plus	Labnet	Cat #08-24-00001-10
Dimethyl sulfoxide	Merck	Cat #D2650
Vectashield	Vector Laboratories	Cat #H-1000
5x Passive Lysis Buffer	Promega	Cat #E1941
VivoGlo™ luciferin	Promega	Cat #P1041
Nuncleon™ Sphera™ low adhesion plates	Thermo Fisher Scientific	Cat #174929
Triton X-100	VWR	Cat #M143
Glycerol	Merck	Cat #G5516
2-mercaptoethanol	Merck	Cat #444233
Nitrocellulose membrane	Cytiva	Cat #15220033
Tween 20	VWR	Cat # M147
SuperSignal™ West Picoplus	Thermo Fisher Scientific	Cat # 34580
cOmplete™ protease inhibitor	Roche	Cat #05892970001
Anti-Flag affinity agarose beads	Merck	Cat #A2220
ANTIBODIES AND RECOMBINANT PROTEINS		
αSMA Rabbit mAb (WB 1:1000)	Cell Signaling Technology	Cat #19245 Clone: D4K9N
β-tubulin Mouse mAb (1:1000)	Cell Signaling Technology	Cat #86298 Clone:D3U1W
β-actin Mouse mAb (WB 1:10000)	Merck	Cat #a1978 Clone:AC-15
Notch2 Rabbit mAb (WB 1:1000)	Cell Signaling Technology	Cat #5732 Clone:D76A6
Notch3 Rabbit mAb (WB 1:1000)	Cell Signaling Technology	Cat #5276 Clone:D11B8
Jagged1 Rabbit mAb (WB 1:1000, ICC 1:100)	Cell Signaling Technology	Cat #2620 Clone:28H8
CD31 Mouse mAb ((ICC 1:100)	Thermo Fisher Scientific	Cat #37-0700 Clone:MEM-05
Pdgfrβ Rabbit mAb (WB 1:1000)	Cell Signaling Technology	Cat #3169 Clone: 2E81
Flag Mouse mAb (WB 1:1000)	Merck	Cat #F1804 Clone: M2

His Rabbit pAb (WB 1:1000)	Cell Signaling Technology	Cat #2365
Phospho Smad2 (Ser465/467) WB Rabbit mAb (WB 1:1000)	Cell Signaling Technology	Cat #3108 Clone:138D4
Smad2/3 (WB 1:200)	Santa Cruz Biotechnology	Cat #sc-133098 Clone:C-8
Anti-Rabbit Goat Ab (WB 1:10000)	Vector Laboratories	Cat #PI-1000
Anti-Mouse Horse Ab (WB 1:10000)	Vector Laboratories	Cat #PI-2000
Veriblot (WB:1:500)	Abcam	Cat #ab131366
Pierce Recombinant Protein G	Thermo Fisher Scientific	Cat #77675
Recombinant human Jagged1-Fc	Bio-techne	Cat #1277-JG
Recombinant human IgG Fc	Bio-Techne	Cat #110-HG
anti-human Alexa fluor 488 antibody	Thermo Fisher Scientific	Cat #21091
anti-rabbit Alexa fluor 488	Thermo Fisher Scientific	Cat #A-11034
anti-mouse Alexa fluor 555	Thermo Fisher Scientific	Cat #A-21422
OLIGONUCLEOTIDES, qPCR PRIMERS, AND PLASMIDS		
siMAX non-targeting control siRNA siControl	Eurofins Genomics	Sequence: 5'-CCU ACA UCC CGA UCG AUG AUG-3'
ON-TARGETplus Human NOTCH2 siRNA -SMARTpool	Horizon Discovery	Cat #L-011093-00-0005
ON-TARGETplus Human NOTCH3 siRNA -SMARTpool	Horizon Discovery	Cat #L-012235-00-0005
ON-TARGETplus Human FOXS1 siRNA -SMARTpool	Horizon Discovery	Cat #L-009029-00-0005
ON-TARGETplus Human SRF siRNA -SMARTpool	Horizon Discovery	Cat #L-009800-00-0005
HCR™ *in situ* hybdridization chain reaction probe for *D. rerio* notch2-x2	Molecular Instruments	NA
HCR™ *in situ* hybdridization chain reaction probe for *D. rerio* notch3-x1	Molecular Instruments	NA

12xCSL-Luciferase	Kato et al. 1997 (https://doi.org/10.1242/dev.124.20.4133)	NA
p3xFlag-CMV	Santio et al., 2016 (https://doi.org/10.18632/oncotarget.9215)	NA
p3xFlag Notch1 ICD CMV		NA
p3xFlag Notch2 ICD CMV		NA
p3xFlag Notch3 ICD CMV		NA
p6xHis-3xGS-RBPJκ CMV	This paper	VectorBuilder ID: VB221019-1188trx
ACTA2, human	TAG Copenhagen	Forward: CGTGTTGCCCCTGAAGAGCAT, Reverse: ACCGCCTGGATAGCCACATACA
HEY1, human	TAG Copenhagen	Forward: TGGATCACCTGAAAATGCTG, Reverse: CGAAATCCCAAACTCCGATA
JAG1, human	TAG Copenhagen	Forward: AATGGCTACCGGTGTGTCTG, Reverse: CCCATGGTGATGCAAGGTCT
NOTCH2, human	TAG Copenhagen	Foward: AAGGAACCTGCTTTGATGACA, Reverse: CAGGGAGCCAATACTGTCTGA
NOTCH3, human	TAG Copenhagen	Forward: CCTAGTCCTGGCTCCGAAC, Reverse: GAGCCGGTTGTCAATCTCC
UBC, human	TAG Copenhagen	Forward: CAC TTG GTC CTG CGC TTG A, Reverse: CAATTGGGAATGCAACAACTTTAT
COL1A1, human	TAG Copenhagen	Forward: GCCAAGACGAAGACATCCCA Reverse: GGCAGTTCTTGGTCTCGTCA
COL4A1, human	TAG Copenhagen	Forward: ACCTGGATTTCAGGGGATGC Reverse: CGGCCTATGAGTCCTGGGTA
Notch2 morpholino	Gene Tools	NA
Notch3 morpholino	Gene Tools	NA
Control morpolino	Gene Tools	NA
SOFTWARE		
Matlab	Mathworks	v.2025a
Image Studio Lite	LI-COR	v.6.0
Prism	Graphpad	v.10

FlowJo	BD Biosciences	v.10
R	NA	v.4.1.0
Seurat	Satija Lab	v.4.4.0
Arivis Vision 4D	Zeiss	v.3.5.0
Imaris	Oxford Instruments	v.10.2.0
Fiji ImageJ	NA	v.2.16.0

1473